

Pion-nucleon scattering in a meson-exchange model

A.M. Gasparyan,^{1,2} J. Haidenbauer,¹ C. Hanhart,¹ and J. Speth¹

¹*Institut für Kernphysik (Theorie), Forschungszentrum
Jülich GmbH, D-52425 Jülich, Germany*

²*Institute of Theoretical and Experimental Physics,
117259, B. Chermushkinskaya 25, Moscow, Russia*

Abstract

The πN interaction is studied within a meson-exchange model and in a coupled-channels approach which includes the channels πN , ηN , as well as three effective $\pi\pi N$ channels namely ρN , $\pi\Delta$, and σN . Starting out from an earlier model of the Jülich group systematic improvements in the dynamics and in some technical aspects are introduced. With the new model an excellent quantitative reproduction of the πN phase shifts and inelasticity parameters in the energy region up to 1.9 GeV and for total angular momenta $J \leq 3/2$ is achieved. Simultaneously, good agreement with data for the total and differential $\pi N \rightarrow \eta N$ transition cross sections is obtained. The connection of the πN dynamics in the S_{11} partial wave with the reaction $\pi N \rightarrow \eta N$ is discussed.

PACS numbers: 14.20.Gk; 13.75.Gx; 11.80.Gw; 24.10.Eq

I. INTRODUCTION

The πN interaction is interesting for several reasons. First, it is one of the main sources of information about the baryon spectrum. Thereby it serves as a doorway to the understanding of QCD in the non-perturbative regime - and especially of the confining mechanism, which is most important for binding a system of quarks into a hadron. For example, experimental information about the mass, width and decay of baryon resonances serves as a testing ground for several models of the internal structure of the nucleon and its excited states. Most of this information is extracted from partial wave analyses of πN scattering data [1, 2, 3].

The πN interaction is also interesting by itself. The wealth of accurate data and the richness of structures shown by them provide an excellent but also challenging testing ground for any model description in terms of effective degrees of freedom, e.g., for chiral perturbation theory [4, 5] but also for the more conventional meson-exchange picture [6, 7, 8].

Finally, the πN interaction is an important ingredient in many other hadronic reactions and in particular for the meson production in nucleon-nucleon (NN) collisions [9, 10]. πN rescattering is an essential mechanism in the reaction $NN \rightarrow NN\pi$ near threshold [11, 12, 13]. There are also strong indications that rescattering involving the πN system plays an important if not dominant role in the production of the η [14, 15, 16, 17] and ω mesons [18, 19] and even for the associated strangeness production ($NN \rightarrow N\Lambda K$, $NN \rightarrow N\Sigma K$) [20, 21]. Thus, model investigations of such production reactions require solid information about the corresponding elementary reactions like $\pi N \rightarrow \eta N$, $\pi N \rightarrow \omega N$, $\pi N \rightarrow K\Lambda$, $\pi N \rightarrow K\Sigma$, etc.

Over the last few years, in a series of papers, the Jülich group has investigated the πN interaction in the meson-exchange framework [8, 22, 23, 24]. One of the main novelties of the model was treating the σ and ρ -meson t -channel exchanges as correlated two-pion exchange, using the dispersion relations technique. The Jülich model was originally constructed to describe elastic πN data not far from threshold [22]. Later the model was extended to higher energies by including several inelastic channels namely three effective $\pi\pi N$ channels (σN , ρN , and $\Delta\pi$) and the ηN channel [8, 24]. The treatment of correlated $\pi\pi$ -exchange was made more consistent and transparent in Ref. [25]. The possibility of generating resonances dynamically was also systematically studied. It turned out, that only one of them, namely the Roper resonance ($P_{11}(1440)$), can be understood in this way in the framework of the Jülich πN model [8, 24]. Other resonances like $S_{11}(1535)$, $S_{11}(1650)$, $D_{13}(1520)$, and $\Delta(1232)$ had to be included explicitly. The latest model provided a good qualitative and in many partial waves even a quantitative description of πN scattering in the energy region from threshold up to 1.9 GeV. [8].

Unfortunately, a further improvement of this model by simply introducing further resonances and by including additional inelastic channels proved to be impossible due to several reasons. First of all, in some partial waves the deviation of the model predictions from the data at higher energies are seemingly not only due to missing resonance contributions. Already the basic (non-resonant or background) contributions of the model by Krehl et al. [8] are incompatible with the general trend exhibited by the experimental phase shifts.

The second problem is a strong influence of the $N^*(1650)$ resonance on the low energy S_{11} phase shift. In fact, it gives the main contribution to this partial wave even at threshold - which is, of course, unphysical. This means, in turn, that any additional channels that couple to the $N^*(1650)$ resonance will likewise have a strong influence on the S_{11} phase shift close to threshold, a certainly undesirable feature.

Finally, the existing πN model yields only an unsatisfactory description of the inelasticity parameter in the S_{11} partial wave and at the same time it overestimates the $\pi N \rightarrow \eta N$ transition cross section close to the ηN threshold. These two related problems are believed to be due to shortcomings in the treatment of the $\pi\pi N$ channel.

In this context, let us mention that the S_{11} partial wave is of particular importance for the ηN and $K\Lambda$ channels close to their thresholds. For $\pi N \rightarrow \eta N$ as well as $\pi N \rightarrow K\Lambda$ experimental information on the transition cross sections and also differential cross sections and polarization observables are available. An analysis of those data within our model requires a satisfactory description of the S_{11} πN partial wave in the relevant energy range. Moreover, an adequate description of the S_{11} inelasticity and of the $\pi N \rightarrow \eta N$ transition amplitude is also needed if one wishes to investigate η production in NN collisions [17]. Similarly, the $\pi N \rightarrow K\Lambda(\Sigma)$ transition amplitude plays an important role in studies of $\Lambda(\Sigma)$ production in NN collisions. It is the main ingredient in the production amplitude based on the pion rescattering mechanism [20].

In the present work we want to remedy the above-mentioned deficiencies of the Jülich πN model [8]. Thereby we aim at a quantitative description of the πN phase shifts and inelasticities for all partial waves with $J \leq 3/2$, from threshold up to around 1.9 GeV. A further and equally important goal is the consistent description of the experimental information on the $\pi N \rightarrow \eta N$ transition.

The paper is structured in the following way: In Sec. II the main ingredients of our πN model are described with special emphasis on those parts of the dynamics where changes and improvements were made. For the time being, apart from the $\pi\pi N$ channel (described effectively via the σN , ρN , and $\Delta\pi$ channels) only the ηN channel is taken into account. However, the inclusion of the $K\Lambda$ channel (and even ωN and $K\Sigma$) is expected to be straightforward within the new improved model. In Sec. III we present results for the πN elastic scattering. Specifically, we compare the πN phase shifts and inelasticities of the new model with experimental values and with the description achieved within the model of Krehl et al. [8]. In addition, and as the main result of our paper we examine in detail the transition reaction $\pi N \rightarrow \eta N$. Calculations for the total transition cross section but also for differential observables are presented. Furthermore, we shed some light on peculiar structures which occur in the $\pi N \rightarrow \eta N$ total cross section of our old model, but also in other models in the literature [26, 27, 28]. The paper ends with a short summary.

II. DESCRIPTION OF THE MODEL

The general framework as well as all technical aspects of the Jülich πN model have been thoroughly described in earlier papers [8, 22, 25]. Therefore, we refrain from repeating all the details here. Rather we want to give a brief account of its main features with specific emphasis on the new and improved ingredients of the present model.

Our model of the πN interaction is derived within the meson-exchange framework in time-ordered perturbation theory (TOPT). Within the envisaged range of validity of our model of up to around 1.9 GeV inelasticities play an increasingly important role, as is evidenced by the results of phase-shift analyses. Hence, coupling to reaction channels that are responsible for those inelasticities have to be taken into account. The decay modes of the nucleon resonances in the energy range under consideration show that the dominant decay (besides πN and ηN for the $N^*(1535)$) is the $\pi\pi N$ channel [29]. Since a three-body calculation is much too complicated for realistic potentials, we represent the $\pi\pi N$ channel

by effective two-body channels. In doing this we are guided by studying strong interactions between two-body clusters of the three-body $\pi\pi N$ state in the spirit of the formalism of Ref. [30]. The dominant clusters are the Δ in the πN interaction, the ρ in the vector-isovector $\pi\pi$ interaction and the strong correlation in the scalar-isoscalar $\pi\pi$ interaction, which we call σ . Therefore – besides the πN and ηN channels – we include in our model the reaction channels $\pi\Delta$, σN and ρN .

Accordingly, we have to solve the coupled-channel scattering equation [31]

$$\begin{aligned} \langle \vec{k}' \lambda_3 \lambda_4 | T_{\mu\nu}^I | \vec{k} \lambda_1 \lambda_2 \rangle &= \langle \vec{k}' \lambda_3 \lambda_4 | V_{\mu\nu}^I | \vec{k} \lambda_1 \lambda_2 \rangle + \\ &\sum_{\gamma} \sum_{\lambda'_1, \lambda'_2} \int d^3q \langle \vec{k}' \lambda_3 \lambda_4 | V_{\mu\gamma}^I | \vec{q} \lambda'_1 \lambda'_2 \rangle \frac{1}{E - W_{\gamma}(q) + i\epsilon} \langle \vec{q} \lambda'_1 \lambda'_2 | T_{\gamma\nu}^I | \vec{k} \lambda_1 \lambda_2 \rangle, \end{aligned} \quad (1)$$

where $\lambda_i, \lambda_{i+2}, \lambda'_i$, ($i = 1, 2$) are the helicities of the baryon and meson in the initial, final and intermediate state, I is the total isospin of the two body system and μ, ν, γ are indices that label different reaction channels. $W_{\gamma}(q) = \sqrt{q^2 + M_{\gamma}^2} + \sqrt{q^2 + m_{\gamma}^2}$ where $m_{\gamma}(M_{\gamma})$ is the mass of the meson (baryon) in the channel γ , respectively. We work in the center-of-momentum (cm) frame and $k(k')$ are the momenta of the initial (final) baryon, respectively.

The pseudopotential $V_{\mu\nu}^I$ (i.e., the interaction between baryon and meson) that is iterated in Eq. (1) is constructed from an effective Lagrangian. Our interaction Lagrangian (see Table I) is based on that of Wess and Zumino [32], which we have supplemented with additional terms for including the Δ isobar, the ω, η, a_0 meson and the σ . We also have included terms that characterize the coupling of the resonances $N^*(1535)$, $N^*(1520)$ and $N^*(1650)$ to various reaction channels. The diagrams that built up the interaction in the $\pi N \rightarrow \pi N$, $\pi N \rightarrow \eta N$, and $\eta N \rightarrow \eta N$ channels are shown in Figs. 1 and 2 as an example and also to introduce our notation. The full set of diagrams, including also the transitions and interactions in the other reaction channels ($\rho N, \sigma N, \pi\Delta$), can be found in Ref. [8]. In that paper one can also find explicit expressions for all the matrix elements $\langle \vec{k}' \lambda_3 \lambda_4 | V_{\mu\nu}^I | \vec{k} \lambda_1 \lambda_2 \rangle$.

As already indicated in the Introduction, there are some modifications and improvements in the present model and we want to summarize them shortly here. First, we now use derivative coupling for the S_{11} N^* resonances, as demanded by chiral symmetry. The corresponding Lagrangians for the $N^*(S_{11})N\pi$ and $N^*(S_{11})N\eta$ vertices can be found in table I. Secondly, we introduce a coupling of the S_{11} $N^*(1535)$ resonance to the $\pi\Delta$ channel. Also this Lagrangian is given in table I. Finally, the subtraction constant that appears in the dispersion relations which constitute the contribution of the correlated $\pi\pi$ exchange in the scalar-isoscalar (σ) channel [22] is not set to zero as in our previous models [8, 24], but allowed to assume a finite value. Interpreted in terms of effective exchanges this contact term corresponds to the exchange of a sigma meson with scalar coupling in addition to the derivative coupling as it occurs now for the sigma exchange stemming from the subtracted dispersion integral. Note, when interpreting the low energy constants c_i , as they occur in the chiral perturbation theory analysis of πN scattering, phenomenologically in terms of resonance exchanges, also both coupling structures of a scalar to pions can be identified [33]. Explicit expressions for those matrix elements $\langle \vec{k}' \lambda_3 \lambda_4 | V_{\mu\nu}^I | \vec{k} \lambda_1 \lambda_2 \rangle$ which differ from the ones employed in our old model [8] can be found in the Appendix.

Mesons and baryons are not point-like particles, but have a finite size. Therefore the interaction vertices mmm and mBB (m =meson, B =Baryon) also have a finite structure which, in our model, is taken into account by means of form factors. Those form factors are parameterized by the following analytical forms, in which \vec{q} is the three momentum transfer

carried by the exchanged particle:

- For meson and baryon exchange

$$F(q) = \left(\frac{\Lambda^2 - m_x^2}{\Lambda^2 + \vec{q}^2} \right)^n. \quad (2)$$

We use monopole form factors ($n = 1$) except for the Δ exchange, for which the convergence of the integral in Eq. (1) requires a dipole form factor ($n = 2$).

- For the nucleon exchange at the πNN vertex

$$F(q) = \frac{\Lambda^2 - m_N^2}{\Lambda^2 - ((m_N^2 - m_\pi^2)/m_N)^2 + \vec{q}^2}. \quad (3)$$

This choice ensures that the nucleon pole and nucleon exchange contribution cancel each other at the Cheng-Dashen point, which is needed for a calculation of the Σ term [22].

- For N , N^* and Δ Pole diagrams

$$F(q) = \left(\frac{\Lambda^4 + m_R^4}{\Lambda^4 + (E_\gamma(q) + \omega_\gamma(q))^4} \right)^n, \quad (4)$$

where $n = 1$ is used for S and P -wave resonances, and $n = 2$ for resonances in higher partial waves.

- The correlated $\pi\pi$ exchange is supplemented by the form factor

$$F(p_2, p_4) = \frac{\Lambda^2}{\Lambda^2 + \vec{p}_2^2} \cdot \frac{\Lambda^2}{\Lambda^2 + \vec{p}_4^2} \quad (5)$$

Note that this choice differs from the form employed in our previous πN models, where the form factor appeared inside the t' integration, cf. Ref. [22]. The particular form we apply in the present work has the following advantages: i) it does not depend on energy; ii) it does not modify strongly the on-shell potential (which is assumed to be fully determined by the dispersion integrals) as long as the energy is not too high; iii) it does not change the t dependence of the potential.

- For the contact interaction in the Wess-Zumino Lagrangian [32]

$$F(p_2, p_4) = \left(\frac{\Lambda^2 + m_4^2}{\Lambda^2 + \vec{p}_4^2} \frac{\Lambda^2 + m_2^2}{\Lambda^2 + \vec{p}_2^2} \right)^2. \quad (6)$$

Finally, we want to emphasize that the Δ isobar in the $\pi\Delta$ channel and the σ and ρ mesons in the σN and ρN channels are not treated as stable particles. Rather, as already mentioned above, the Δ , σ and ρ here stand for πN and $\pi\pi$ subsystems with the quantum numbers of the P_{33} partial wave in the πN system and the $I = J = 0$ and $I = J = 1$ partial waves in the $\pi\pi$ system, respectively. In order to simulate these, a simplified model for the P_{33} πN partial wave as well as for the δ_{00} and δ_{11} $\pi\pi$ partial waves was adopted in which pole diagrams, in the framework of time-ordered perturbation theory, are iterated [8, 24].

These models are then used to construct the self-energies of the Δ , σ and ρ which appear in the propagators of the $\pi\Delta$ and σN intermediate states in our scattering equation, i.e. we replace the two-particle intermediate state propagator for $\pi\Delta$, σN and ρN by

$$\frac{1}{E - W_\gamma(q)} \rightarrow \frac{1}{E - W_\gamma(q) - \Sigma_\gamma(E_{sub})}, \quad (7)$$

where

$$\begin{aligned} E_{sub} &= E - \omega_\pi(q) - (\sqrt{(M_\Delta^o)^2 + q^2} - M_\Delta^o) \text{ for the } \Delta, \\ E_{sub} &= E - E_N(q) - (\sqrt{(m_r^o)^2 + q^2} - m_r^o) \text{ for } r = \rho, \sigma \end{aligned} \quad (8)$$

is the energy of the decaying cluster at rest [24]. The bare masses M_Δ^o and m_r^o are determined by fitting the models to the relevant phase shifts of the πN and $\pi\pi$ systems, cf. Refs. [24] and [8] for details. By taking into account the self-energy contributions we preserve the correct threshold behavior for the description of pion production in the πN system.

The scattering equation (1) is reduced to a set of one-dimensional intergral equations by means of the usual partial wave decomposition [34] and then solved numerically by standard contour-deformation methods [35, 36].

III. RESULTS

In this section we present the results of our model for πN elastic scattering and for the $\pi N \rightarrow \pi\eta$ transition in the energy range from πN threshold up to 1.9 GeV. First we discuss the parameters that enter into our model calculation. Then we present the results for the πN phase shifts and inelasticities. In particular, the role of the background and of the resonance contributions is analyzed. We also compare the results with those of the previous version of the model. Furthermore, we analyse in detail the results for the $\pi N \rightarrow \eta N$ total cross section and angular distributions and discuss the role of the background in this process.

A. Parameters of the model

Our model is based on the effective potential, which was described in section II.

The masses of all the particles appearing in the model are collected in table II. Here one should pay attention to the mass of the σ meson. While the σ exchange in the $\pi N \rightarrow \pi N$ potential is evaluated using a dispersion relation, we have another t -channel σ exchange in the $\sigma N \rightarrow \sigma N$ potential. In this case we choose the value $m_\sigma = 650$ MeV, which was extracted from a Breit-Wigner parameterization of the correlated $\pi\pi$ -exchange in Ref. [37].

Table A 1 contains coupling constants and cutoff parameters of the form factors for the vertices entering the t and u -exchange diagrams and the contact terms, i.e. those, which constitute the background.

Most of the coupling constants have been taken from other sources. The coupling constants of the pole diagrams are constrained by values determined from their decay widths, for which we take the estimates of Ref. [38]. The parameters which are not fixed from other sources are shown in boldface. These are the purely phenomenological coupling constant at the triple σ vertex, $g_{\sigma\sigma\sigma}$, and the subtraction constant A_0 for the dispersion relation in

the σ channel. In addition the cutoff masses are treated as free parameters. Those free parameters are determined by a fit to the πN phase shifts and inelasticities for $J \leq 3/2$ and the $\pi N \rightarrow \eta N$ cross section in the energy range from threshold to about 1.9 GeV. Here we should emphasize that we restrict ourselves to values of the cutoff masses of about 1-1.5 GeV (in some cases up to 2 GeV for heavy exchanged particles), i.e. values in line with typical hadronic scales.

Parameters of the pole diagrams (bare masses and coupling constants) are given in table IV. Note that the bare nucleon mass and bare πN coupling constant $f_{\pi NN}^B$ are not free parameters, because they are fixed by the physical values of these quantities (cf. Ref. [22]). However, the cutoff at the πNN vertex was allowed to vary, in order to fit the P_{11} partial wave. The resulting parameters for the nucleon pole are:

$$M_0 = 1239 \text{ MeV}, \quad \frac{(f_{NN\pi}^B)^2}{4\pi} = 0.0166, \quad \Lambda = 1950 \text{ MeV}. \quad (9)$$

The cutoff masses for all other resonance diagrams were set to 2 GeV. Indeed the results depend only weakly on the particular values of the cutoff masses, since their effects can be always compensated by a change in the corresponding coupling constants. The largeness of the cutoff masses in the resonance diagrams is motivated by the specific analytical form of the employed resonance form factors, which fall off with momentum rather rapidly even for such a large cutoff mass [39].

In general we adopt positive values for the sign of the bare coupling constants. However, we use negative coupling constants if this leads to a better agreement with the data. In the case of the $N_{P_{13}}^*(1720)\eta N$ vertex we changed the sign of the coupling constant because that allow to obtain a better description of the $\pi N \rightarrow \eta N$ differential cross section via an interference of the P_{13} with other partial waves. Finally, we would like to remark that among the three phase shift analyses whose results are shown in figures we use the energy independent analysis from Ref. [2] as main guideline for the fitting procedure.

B. πN elastic scattering

We start the discussion of the elastic πN data by first looking at the phase shifts as they result from the original model of O. Krehl et al. [8] (cf. the dashed curves in figs. 3 and 4). In general, the quality of the description is rather good, but there are some unsatisfactory features which we would like to point out here.

First, there are significant deviations of the model results from the data in some partial waves, specifically in the P_{13} , S_{31} , and D_{33} waves. Evidently, the discrepancies are primarily due to the presence of resonances in these partial waves, which are not yet included in the model. However, it is easy to see, that the inclusion of the resonances in question alone will not help in the case of P_{13} and S_{31} . This is because such resonance contributions will vanish again above the position of the resonance within the energy range given roughly by the width and the phase shift will change by 180° (if the resonance contribution and the background have the same signs) or turn back to the background (if they have opposite signs). However, as one can see from figs. 3 and 4, in the P_{13} partial wave the phase goes in opposite direction to the data, and in S_{31} partial wave the deviation from the data at energies above the position of the resonance is huge.

The second problem of the πN model of Krehl et al. is the presence of a long tail of the $S_{11}(1650)$ resonance. This leads to the undesirable feature, that even at very low

energies the S_{11} phase shift is strongly influenced by this resonance – in conflict with chiral symmetry. As was shown by Weinberg and Tomozawa [40, 41] the isovector s -wave πN scattering length is fully determined to leading order by the pion mass m_π and pion decay constant F_π . Therefore, the presence of contributions related to the $N^*(1650)$ resonance at low energies is unnatural and physically hard to justify. Fig. 6 shows the discussed effect. One can see that the low energy S_{11} phase shift even changes its sign when all couplings to the $S_{11}(1650)$ resonance are switched off.

A detailed inspection of this problem revealed that the long tail of the $S_{11}(1650)$ resonance is predominantly due to the rather hard form factors used in the model of Krehl et al. and, in particular, in those diagrams contributing to the $\pi N \rightarrow \rho N$ transition potential (there is a direct coupling of the ρN channel to the $S_{11}(1650)$). As was mentioned before, in the new model we want to avoid the use of extremely large cutoff masses anyway. A further reduction of the near threshold contribution from the $S_{11}(1650)$ resonance is achieved by choosing the derivative coupling for the $N_{S_{11}}^* N \pi$ vertex (see appendix A) in analogy with the $NN\pi$ coupling. In the new model the missing strength at low energies is provided by the correlated $\pi\pi$ -exchange in the σ -channel. It can be generated by allowing the subtraction constant, which occurs in the corresponding dispersion relations, cf. Eq. (31) in Ref. [22], and which was set to zero by hand in the old model [8], to assume a finite but still small value.

Now, let us consider the non-resonant part (or the background) of the new model. First one should note that the main contribution to the background at low energies is, of course, provided by diagrams that involve only the πN channel. Therefore, we start by discussing the importance of various πN graphs for the different partial waves. There are five diagrams in the $\pi N \rightarrow \pi N$ potential, cf. Fig. 1a-e: correlated $\pi\pi$ exchange in the $J = 0, I = 0$ (σ) and $J = 1, I = 1$ (ρ) channels, nucleon and Δ u -channel exchanges, and the nucleon (s -channel) pole diagram. It turned out that the contribution from the Δ -exchange is very small in all partial waves. (As a consequence of that, we do not include u -channel graphs involving heavier resonances!) The S waves are dominated by the ρ and σ exchanges. The nucleon exchange becomes important in higher partial waves. Note also, that the ρ -exchange alone provides such a strong attraction in the P_{11} partial wave that it is almost sufficient for the formation of a resonance. However, it is partly cancelled by the contribution from the nucleon pole. One should emphasize here that, in contrast to the old model, we do not have much freedom in varying the strength of the ρ and σ exchanges (except for the subtraction constant mentioned above) since their contributions at low energies are basically fixed due to our choice of the form factors (see section II). Thus, the simultaneous description of the background in seven partial waves with a rather small number of parameters is to be considered as a success of our model (cf. dash-dotted lines in fig. 3 and fig. 4). We have not included the P_{11} partial wave in these consideration, because there the coupling to the σN channel plays a rather important role.

As a confirmation for the quality of the background contribution we also looked at the phase shifts with $J = 5/2$, cf. Fig. 5. Those partial waves were not include in the fitting procedure and, therefore, are genuine predictions of our model. It is evident that our results are quite in line with the general trend of the data (disregarding the resonance structures, of course).

The next step is the inclusion of the inelastic channels. The most important ones are those that represent effectively the $\pi\pi N$ channel, namely ρN , σN and $\pi\Delta$. The σN channel couples dominantly to the P_{11} πN partial wave. It is a consequence of the parity difference

between π and σ , which implies that the P_{11} πN partial wave couples to an S wave in the σN system. In the course of adjusting the free parameters attraction is introduced into the σN channel and also a strong $\pi N \rightarrow \sigma N$ transition potential results. This, in turn, provides additional attraction in the πN channel via coupled-channels effects and eventually leads to a dynamical generation of the $N^*(1440)$ (Roper) resonance in the P_{11} partial wave. This mechanism and also its implications for the Roper resonance were discussed extensively in previous studies [8, 24] by the Jülich group and therefore we do not repeat the arguments here. However, it is certainly reassuring that also within the new model the Roper resonance turns out to be dynamically generated and no genuine $N^*(1440)$ (three quark) resonance is needed in order to explain the P_{11} partial wave.

The channels ρN and $\pi\Delta$ are important for the inelasticities at high energies in all partial waves, but in particular in the D_{13} , P_{31} , and P_{33} . In the P_{33} partial wave there are no resonances in this energy region that couple strongly to the πN system [29]. Thus, coupling to those channels via t - and u -channel exchange diagrams is the only source of inelasticity in the P_{33} πN partial wave. The most important diagrams for the P_{33} inelasticity are the ρ -exchange in the $\pi N \rightarrow \pi\Delta$ potential and, partly, the nucleon exchange in the $\pi N \rightarrow \rho N$ potential. One should mention here also the π -exchange diagram in the $\pi N \rightarrow \rho N$ transition. It turns out to be much too strong in the P_{13} and S_{11} partial waves, independently of the cutoff used. Its contribution alone produces a very strong cusp in the region of the ρN threshold in the S_{11} phase shift, and drastically modifies the behavior of the P_{13} phase shift, bending it upwards. Luckily the π -exchange contribution is cancelled to a large extent by the $\pi N \rightarrow \rho N$ contact term from the Wess-Zumino Lagrangian, and also by the ω -exchange diagram. Ultimately, on the whole the phase shifts are not too much affected by the inelastic channels.

The final step in the description of the elastic πN data consists in adding the resonance terms. We included resonances in all partial waves except for the P_{11} where our model reproduces the phase shift and inelasticity, including the structure associated with the Roper resonance, dynamically via a strong coupling to the σN channel, as mentioned already above. In the S_{11} partial wave there are two resonances, namely the $N^*(1535)$ and the $N^*(1650)$. The former dominates the near threshold $\pi N \rightarrow \eta N$ cross section. (The ηN channel will be discussed in detail in the next subsection.) As can be seen from the parameters given in table IV, among the effective $\pi\pi N$ channels, the $\pi\Delta$ channel is allowed to couple to most of the resonances. This channel becomes relevant already at rather low energies (in contrast to the ρN channel) and it can contribute to both ($I = 1/2$ and $I = 3/2$) isospin states. Since we cannot calculate $\pi N \rightarrow \pi\pi N$ observables directly at the moment (due to technical difficulties that arise from 3-body singularities) – which would allow to further constrain the relative importance of the different $\pi\pi N$ channels – we choose this particular channel for describing the bulk of the $\pi\pi N$ part of the πN inelasticity. However, in addition the ρN channel needs to be coupled to some resonances namely to $D_{13}(1520)$, $S_{11}(1650)$, and $D_{33}(1700)$. In those cases the different energy behavior resulting from the ρN channel is required for a satisfactory description of the experimental phase shifts as well as the inelasticities.

The position of the $P_{31}(1910)$ resonance is located already above the energy region we are interested in (which is from πN threshold up to ~ 1.9 GeV). Nevertheless it was included because its tail still influences noticeably the energy region around $1.8 \sim 1.9$ GeV.

Note that, among others, the inelasticity in the P_{13} partial wave shows an incorrect trend at higher energies, and the data are underestimated. A similar, but less pronounced

deficiency can be found in the D_{13} inelasticity. Some authors claim, that there is a sizable contribution from the ωN channel, which opens at around 1.7 GeV, to these particular partial waves [42]. Therefore, the inclusion of the ωN channel might improve the description of these data.

Finally, let us mention that also the low energy parameters of πN scattering are in reasonable agreement with available data, as it should be, since we fit our model to the phase shift analyses. The S and P -wave scattering lengths and volumes are collected in table V.

C. Description of the ηN channel

The reaction $\pi N \rightarrow \eta N$ near the ηN threshold is closely related to the properties of the $N^*(1535)$ resonance. The total cross section of this reaction has a very pronounced peak structure at the position of the resonance (cf. Fig. 7). In the previous version of the Jülich πN model the total $\pi^- p \rightarrow \eta n$ cross section was overestimated by about 20-30% around the maximum. The reason for this deficiency is that only the πN and ηN channels were allowed to couple to the $N^*(1535)$ resonance. Therefore, in order to describe the S_{11} πN amplitude one had to generate basically the whole inelasticity in this partial wave by the coupling to the ηN channel. Indeed the contribution of the S_{11} partial wave to the inelastic $\pi^- p$ cross section is given by

$$\sigma_{in} = \frac{2\pi}{3k_1^2}(1 - \eta^2), \quad (10)$$

which amounts to $\sigma_{in} \sim 3.5$ mb at the maximum using the inelasticity η as given by the phase shift analysis. However, the experimental $\pi^- p \rightarrow \eta n$ cross section is always below 3 mb, cf. Fig. 7. Thus, it is clear that there must be contributions of other channels to the S_{11} inelasticity. The only other channel which is open at energies around the η threshold is the $\pi\pi N$ channel. Indeed the $\pi\pi N$ channel was found to be important in an analysis of the πN S-waves within the chiral unitary approach of Inoue et al. [43]. Accordingly, we introduce a coupling of the $\pi\Delta$ system – which in our model is one of the effective channels that represent the $\pi\pi N$ channel – to the $N^*(1535)$ resonance. This enables us to describe simultaneously the total $\pi^- p \rightarrow \eta n$ cross section and the inelasticity in the S_{11} partial wave in the resonance region, as can be seen in Figs. 7 and 3, respectively.

The inclusion of an $N^*\Delta\pi$ coupling improves also the description of the S_{11} inelasticity above the position of the $N^*(1535)$ resonance. In Fig. 3 one can see that the old Jülich model produces a strong dip in the S_{11} inelasticity, which then leads to a similar dip in the S -wave $\pi^- p \rightarrow \eta n$ cross section. We found that the origin of this behavior is essentially a unitarity constraint from the πN channel. It can be easily understood schematically, if we assume a two-channel problem involving only the πN and ηN systems. We also assume that, apart from the $N^*(1535)$ resonance (whose contribution drops quickly when one moves away from its peak) there is some background contribution to the $\pi N \rightarrow \eta N$ transition potential and that at the same time (which is the crucial point) the direct $\eta N \rightarrow \eta N$ potential is negligibly small. (These conditions are satisfied in the old Jülich model.) Then the $\pi N \rightarrow \eta N$ T -matrix (we consider only the S_{11} partial wave) is given by

$$T_{\pi N \rightarrow \eta N} = V_{\pi N \rightarrow \eta N}(1 + G_0 T_{\pi N \rightarrow \pi N}), \quad (11)$$

which can be re-expressed in the form (see, e.g., Ref. [44])

$$T_{\pi N \rightarrow \eta N} = (1 + (\beta + ik_{\pi N}) \frac{\eta e^{2i\delta} - 1}{2ik_{\pi N}}) V_{\pi N \rightarrow \eta N}. \quad (12)$$

Here β is the inverse of the characteristic range of interaction, which is determined by the principal value integral, δ and η are the S_{11} phase shift and inelasticity parameter and $k_{\pi N}$ is the on-shell momentum in the πN channel. Let us now examine under what circumstances we can have $T_{\pi N \rightarrow \eta N} = 0$. Given our simplifying model assumption, the condition $T_{\pi N \rightarrow \eta N} = 0$ implies that $\eta = 1$, and consequently β is purely real. Then, it is convenient to rewrite Eq. (12) as

$$T_{\pi N \rightarrow \eta N} = e^{i\delta} \sqrt{1 + \beta^2/k_{\pi N}^2} \sin(\gamma - \alpha) V_{\pi N \rightarrow \eta N}, \quad (13)$$

where $\gamma = \arctan(\beta/k_{\pi N})$ and $\alpha = \delta - \pi/2$. Note that in the specific situation we discuss the phase δ crosses $\pi/2$ ($\alpha = 0$), due to the presence of the $N^*(1650)$ resonance in the $\pi N \rightarrow \pi N$ interaction, and then continues to rise rapidly, whereas β is a smooth function of $k_{\pi N}$ and has a typical value in the order of several hundreds MeV (the exact value is, of course, model dependent), so that in the region of interest we have $\gamma \lesssim 1$. It is thus easy to convince oneself that the expression in Eq. (13) equals zero at some energy above (but not far from) the position of the $N^*(1650)$ resonance. Expanding $T_{\pi N \rightarrow \eta N}$ in powers of $Z - Z_0$, where Z_0 is the position of the “zero”, one can see that the $\pi^- p \rightarrow \eta n$ cross section is proportional to $(Z - Z_0)^2$ - which explains the structure of the dip in the cross section exhibited by the old Jülich model (dotted line in Fig. 7). It is interesting to note that the same effect can be found in other model analyses, e.g. in the ones by Gridnev and Kozlenko [26] and by the Giessen group [27, 28]. In general, when there are more than two channels, β becomes complex and the cross section at the dip will be finite - but it will be still small (provided that the inelasticity is not too large).

In our model the S_{11} inelasticity in the energy region around the η threshold is partly determined by the $N^*(1535)\Delta\pi$ coupling. In the $\Delta\pi$ system this resonance couples to a pure D -wave. Because of that the maximum of the $\pi N \rightarrow \pi\Delta$ transition cross section is shifted to somewhat higher energies as compared to the resonance energy. Its contribution to the inelasticity is likewise shifted to somewhat higher energies and fills up the dip that can be seen in the S_{11} inelasticity predicted by the old model, cf. Fig. 3. It also smoothens out the effect discussed above and, therefore, we can achieve a fairly realistic description of the energy dependence of $\sigma_{\pi^- p \rightarrow \eta n}$ over the region of the $N^*(1650)$ resonance. Specifically, we don't get this strong double hump structure prominently visible in the model analysis of Ref. [27], cf. their Fig. 7.

Let us now look at the energy dependence of the total cross section over a wider energy range and also at the $\pi^- p \rightarrow \eta n$ differential cross section in order to examine the importance of higher partial waves. To include the effect of higher partial waves we introduced a coupling of the ηN system to the $P_{13}(1720)$ and $D_{13}(1520)$ resonances. Those are the most pronounced resonances in the energy region below 1.9 GeV that couple strongly to the πN system. Note that there are other 3-star N^* resonances [29] in this region. However, we do not include those because their coupling to the πN channel is very weak and therefore their parameters cannot be sufficiently constrained from the πN data.

At energies below 1.6 GeV the slight deviation of the differential cross section from the isotropic distribution can be easily described by the interference of the D_{13} resonance with

the S -wave amplitude [45], cf. fig. 8. For the total cross section the D_{13} contribution is of minor importance. Above 1.6 GeV the total cross section can be described by introducing a coupling of the ηN system to the $P_{13}(1720)$ resonance as is evidenced by the results shown in fig. 7. However, as is obvious from fig. 9, this coupling alone is not sufficient to achieve also good agreement with the data for the differential cross section in this energy region. Most likely that points to missing contributions from higher partial waves, and specifically from $J = 5/2$ resonances. At present we do not aim to include those. We would like to remark also that the existing data do not allow one to discriminate between different partial-wave contributions – one would need to know polarization observables for this purpose.

Finally, we want to draw attention to the fact that in our model there is also a background contribution to the $\pi N \rightarrow \eta N$ transition interaction which is provided by t -channel exchange of the $a_0(980)$ meson, cf. Fig. 2b. However, the role of a_0 exchange is now strongly reduced as compared to the old Jülich model, mainly because in the present model we avoid large values of the cutoff mass. In any case, the influence of the $a_0(980)$ meson is suppressed at energies above the $N^*(1535)$ resonance due to the mechanism discussed above.

We also want to present the ηN effective range parameters predicted by our model. They are

$$\begin{aligned} a_{\eta N} &= (0.41 + i0.26)fm, \\ r_{\eta N} &= (-3.4 + i0.4)fm. \end{aligned} \tag{14}$$

Obviously, our result for $\text{Re}(a_{\eta N})$ is at the lower end of the spectrum of values that one can find in the literature, cf., e.g., the compilation given in Table 1 of Ref. [46]. In fact, it is even slightly lower than the one of the old Jülich model, which yields $a_{\eta N} = (0.42 + i0.34)$ fm. However, we want to emphasize that such a value is pretty much in line with conclusions drawn from recent analyses of the ηN final state interaction in the reactions $\gamma d \rightarrow np\eta$ [46] and $pn \rightarrow d\eta$ [47, 48].

IV. SUMMARY

We have presented results of an extended and improved version of the Jülich πN model. The model is based on the meson exchange picture and it is derived in its main part from the phenomenological Wess-Zumino Lagrangian, consistent with chiral symmetry. The πN interaction in the scalar-isoscalar and vector-isovector channels is calculated by means of dispersion relations from correlated $\pi\pi$ exchange in order to constrain the contributions of the corresponding σ and ρ exchanges. In the present work ambiguities in the treatment of dispersion relations (cf. sect. IIIB of Ref. [22]) are even further reduced by a choice of the form factors that does not modify the strength and t dependence of the interaction at low energies. In addition some more improvements have been implemented. In particular, we now use derivative coupling for the S_{11} N^* resonances at the πN and ηN vertices, as is demanded by chiral symmetry anyway. We also include some more resonance diagrams, specifically for the $S_{13}(1620)$, $P_{13}(1720)$, $P_{13}(1910)$, $D_{13}(1520)$, and $D_{33}(1700)$ resonances.

The potential constructed in this way was unitarized in a coupled channels Lippmann-Schwinger equation to obtain the reaction amplitudes for various processes. The reaction channels included in the present investigation are πN , ηN , σN , ρN , and $\pi\Delta$, where the latter three channels are understood as an effective description of the physical $\pi\pi N$ state.

With the new model an excellent quantitative reproduction of the πN phase shifts and inelasticity parameters in the energy region up to 1.9 GeV and for total angular momenta

$J \leq 3/2$ was achieved. In addition a good description of the background in the $J = 5/2$ partial waves was obtained automatically. As far as the P_{11} partial wave is concerned we confirm the results of our earlier investigations that the structure associated with the Roper resonance is generated dynamically by the model so that no genuine $N^*(1440)$ (three quark) resonance diagram needs to be included.

As the main new aspect we studied in detail the coupling of the πN system to the ηN channel. First of all we showed that the overestimation of the $\pi^- p \rightarrow \eta n$ cross section in the region of the $N^*(1535)$ resonance by the old Jülich model can be removed by introducing additional flux from the πN to the $\pi \Delta$ channel. Furthermore, the inclusion of the ηN coupling to the $P_{13}(1720)$ resonance turned out to lead to a significant improvement of the total cross section at higher energies. At the same time the puzzle of the dip in the S_{11} inelasticity, present in the old Jülich model but also in other models in the literature [26, 27], could be explained. The origin of this deficiency turned out to be an almost model independent effect of coupled-channels unitarity constraints. We also improved the description of the $\pi^- p \rightarrow \eta n$ differential cross section. A remaining discrepancy with the data at higher energies is most likely caused by contributions from partial waves with $J > 3/2$ which are not included in our model calculation. Note, that a detailed partial wave analysis of this reaction at such energies is presently impossible because of the lack of data on polarization observables.

The model in its present form enables a straightforward inclusion of further reaction channels, and specifically those nearest in energy namely $K\Lambda$, $K\Sigma$, and ωN . Such an extension of the present model in this direction is planned for the future.

Acknowledgments

We thank S. Krewald and I.R. Afnan for stimulating discussions.

APPENDIX A: THE PSEUDOPOTENTIAL

In this appendix we give the expressions for those contributions to the interaction potentials that differ from our earlier work [8]. For convenience we also summarize here all pole diagrams since most of them were not included in the old model. All other expressions for the pseudopotential can be found in Appendix A of Ref. [8]. The notation for the different particles and their momenta is given in Fig. 1. E_1 , E_3 , ω_2 and ω_4 indicate on-mass-shell-energies of baryons 1 and 3 and, respectively those of mesons 2 und 4:

$$E_i = \sqrt{m_i^2 + \vec{p}_i^2} \quad ; \quad \omega_i = \sqrt{m_i^2 + \vec{p}_i^2} \quad . \quad (\text{A1})$$

q is the four-momentum of the intermediate particle. The tensor operator $P^{\mu\nu}$ is given in Eq. (A12) of Ref. [8].

Since we work in time-ordered perturbation theory, all the potentials contain the normalization factor

$$\kappa = \frac{1}{(2\pi)^3} \sqrt{\frac{m_1 m_3}{E_1 E_3}} \sqrt{\frac{1}{2\omega_2 2\omega_4}} \quad . \quad (\text{A2})$$

1. $\pi N \rightarrow \pi N$

- correlated $\pi\pi$ exchange in the σ channel (Fig. 1c)

$$-\kappa \bar{u}(\vec{p}_3, \lambda_3) u(\vec{p}_1, \lambda_1) \left[A_0 + 16(-2p_{2\mu} p_4^\mu) \int dt' \frac{\text{Im}(f_+^0(t'))}{(t' - 2m_\pi^2)(t' - 4m_N^2)} P(t') \right] IF_{\sigma t}(I), \quad (\text{A3})$$

where $P(t') = \frac{1}{2\omega_{t'}} \left(\frac{1}{E - \omega_2 - E_3 - \omega_{t'}} + \frac{1}{E - \omega_4 - E_1 - \omega_{t'}} \right)$, $\omega_{t'} = \sqrt{q^2 + t'}$ and f is a Frazer-Fulco amplitude [25, 49]. The isospin coefficients are equal to $IF_{\sigma t}(1/2) = 1$, $IF_{\sigma t}(3/2) = 1$.

- $N^*(S_{11}, S_{31})$ pole diagrams (Fig. 1g)

$$\kappa \frac{f_{N^*N\pi}^2}{m_\pi^2} \bar{u}(\vec{p}_3, \lambda_3) \not{p}_4 \frac{1}{2m_{N^*}^0} \frac{\not{q} + m_{N^*}^0}{E - m_{N^*}^0} \not{p}_2 u(\vec{p}_1, \lambda_1) IF_{N^*s}(I). \quad (\text{A4})$$

- Nucleon, $N^*(P_{31})$ pole diagrams

$$\kappa \frac{f_{N^*N\pi}^2}{m_\pi^2} \bar{u}(\vec{p}_3, \lambda_3) \gamma^5 \not{p}_4 \frac{1}{2m_{N^*}^0} \frac{\not{q} + m_{N^*}^0}{E - m_{N^*}^0} \gamma^5 \not{p}_2 u(\vec{p}_1, \lambda_1) IF_{N^*s}(I). \quad (\text{A5})$$

- $N^*(P_{13}, P_{33})$ pole diagrams

$$\kappa \frac{f_{N^*N\pi}^2}{m_\pi^2} \bar{u}(\vec{p}_3, \lambda_3) p_{4\mu} \frac{1}{2m_{N^*}^0} \frac{P^{\mu\nu}(q)}{E - m_{N^*}^0} p_{2\nu} u(\vec{p}_1, \lambda_1) IF_{N^*s}(I). \quad (\text{A6})$$

- $N^*(D_{13}, D_{33})$ pole diagrams

$$\kappa \frac{f_{N^*N\pi}^2}{m_\pi^4} \bar{u}(\vec{p}_3, \lambda_3) \gamma^5 \not{p}_4 p_{4\mu} \frac{1}{2m_{N^*}^0} \frac{P^{\mu\nu}(q)}{E - m_{N^*}^0} \gamma^5 \not{p}_2 p_{2\nu} u(\vec{p}_1, \lambda_1) IF_{N^*s}(I). \quad (\text{A7})$$

$$IF_{N^*s}(1/2) = 3, IF_{N^*s}(3/2) = 1.$$

2. $\pi N \rightarrow \eta N$

- $N^*(S_{11})$ pole diagram

$$\kappa \frac{f_{N^*N\pi} f_{N^*N\eta}}{m_\pi^2} \bar{u}(\vec{p}_3, \lambda_3) \not{p}_4 \frac{1}{2m_{N^*}^0} \frac{\not{q} + m_{N^*}^0}{E - m_{N^*}^0} \not{p}_2 u(\vec{p}_1, \lambda_1) IF_{N^*s}(I). \quad (\text{A8})$$

- $N^*(P_{13})$ pole diagram

$$\kappa \frac{f_{N^*N\pi} f_{N^*N\eta}}{m_\pi^2} \bar{u}(\vec{p}_3, \lambda_3) p_{4\mu} \frac{1}{2m_{N^*}^0} \frac{P^{\mu\nu}(q)}{E - m_{N^*}^0} p_{2\nu} u(\vec{p}_1, \lambda_1) IF_{N^*s}(I). \quad (\text{A9})$$

- $N^*(D_{13})$ pole diagram

$$\kappa \frac{f_{N^*N\pi} f_{N^*N\eta}}{m_\pi^4} \bar{u}(\vec{p}_3, \lambda_3) \gamma^5 \not{p}_4 p_{4\mu} \frac{1}{2m_{N^*}^0} \frac{P^{\mu\nu}(q)}{E - m_{N^*}^0} \gamma^5 \not{p}_2 p_{2\nu} u(\vec{p}_1, \lambda_1) IF_{N^*s}(I). \quad (\text{A10})$$

$$IF_{N^*s}(1/2) = \sqrt{3}.$$

3. $\pi N \rightarrow \rho N$

- $N^*(S_{11})$ pole diagram

$$-i\kappa \frac{f_{N^*N\pi} g_{N^*N\rho}}{m_\pi} \bar{u}(\vec{p}_3, \lambda_3) \gamma^5 \xi^*(\vec{p}_4, \lambda_4) \frac{1}{2m_{N^*}^0} \frac{\not{q} + m_{N^*}^0}{E - m_{N^*}^0} \not{p}_2 u(\vec{p}_1, \lambda_1) IF_{N^*s}(I). \quad (\text{A11})$$

- $N^*(D_{13}, D_{33})$ pole diagrams

$$i\kappa \frac{f_{N^*N\pi} f_{N^*N\rho}}{m_\pi^2 m_\rho} \bar{u}(\vec{p}_3, \lambda_3) (\not{p}_4 \epsilon_\mu^*(\vec{p}_4, \lambda_4) - p_{4\mu} \not{\epsilon}^*(\vec{p}_4, \lambda_4)) \\ \times \frac{P^{\mu\nu}(q)}{2m_{N^*}(E - m_{N^*}^0)} p_{2\nu} \gamma^5 \not{p}_2 u(\vec{p}_1, \lambda_1) IF_{N^*s}(I) \quad (\text{A12})$$

$$IF_{N^*s}(1/2) = 3, IF_{N^*s}(3/2) = 1.$$

4. $\pi N \rightarrow \pi \Delta$

- $N^*(S_{11}, S_{31})$ pole diagrams

$$\kappa \frac{f_{N^*N\pi} f_{N^*\Delta\pi}}{m_\pi^2} \bar{u}_\mu(\vec{p}_3, \lambda_3) p_4^\mu \gamma^5 \frac{1}{2m_{N^*}^0} \frac{\not{q} + m_{N^*}^0}{E - m_{N^*}^0} \not{p}_2 u(\vec{p}_1, \lambda_1) IF_{N^*s}(I). \quad (\text{A13})$$

- $N^*(P_{31})$ pole diagram

$$\kappa \frac{f_{N^*N\pi} f_{N^*\Delta\pi}}{m_\pi^2} \bar{u}_\mu(\vec{p}_3, \lambda_3) p_4^\mu \frac{1}{2m_{N^*}^0} \frac{\not{q} + m_{N^*}^0}{E - m_{N^*}^0} \gamma^5 \not{p}_2 u(\vec{p}_1, \lambda_1) IF_{N^*s}(I). \quad (\text{A14})$$

- $N^*(P_{13})$ pole diagram

$$\kappa \frac{f_{N^*N\pi} f_{N^*\Delta\pi}}{m_\pi^2} \bar{u}_\mu(\vec{p}_3, \lambda_3) \gamma^5 \not{p}_4 \frac{1}{2m_{N^*}^0} \frac{P^{\mu\nu}(q)}{E - m_{N^*}^0} p_{2\nu} u(\vec{p}_1, \lambda_1) IF_{N^*s}(I). \quad (\text{A15})$$

- $N^*(D_{13}, D_{33})$ pole diagrams

$$-\kappa \frac{f_{N^*N\pi} f_{N^*\Delta\pi}}{m_\pi^3} \bar{u}_\mu(\vec{p}_3, \lambda_3) \not{p}_4 \frac{1}{2m_{N^*}^0} \frac{P^{\mu\nu}(q)}{E - m_{N^*}^0} \gamma^5 \not{p}_2 p_{2\nu} u(\vec{p}_1, \lambda_1) IF_{N^*s}(I). \quad (\text{A16})$$

$$IF_{N^*s}(1/2) = -\sqrt{6}, IF_{N^*s}(3/2) = \sqrt{\frac{5}{3}}.$$

5. $\eta N \rightarrow \eta N$

- $N^*(S_{11})$ pole diagram

$$\kappa \frac{f_{N^*N\eta}^2}{m_\pi^2} \bar{u}(\vec{p}_3, \lambda_3) \not{p}_4 \frac{1}{2m_{N^*}^0} \frac{\not{q} + m_{N^*}^0}{E - m_{N^*}^0} \not{p}_2 u(\vec{p}_1, \lambda_1) IF_{N^*s}(I). \quad (\text{A17})$$

- $N^*(P_{13})$ pole diagram

$$\kappa \frac{f_{N^*N\eta}^2}{m_\pi^2} \bar{u}(\vec{p}_3, \lambda_3) p_{4\mu} \frac{1}{2m_{N^*}^0} \frac{P^{\mu\nu}(q)}{E - m_{N^*}^0} p_{2\nu} u(\vec{p}_1, \lambda_1) IF_{N^*s}(I). \quad (\text{A18})$$

- $N^*(D_{13})$ pole diagram

$$\kappa \frac{f_{N^*N\eta}^2}{m_\pi^4} \bar{u}(\vec{p}_3, \lambda_3) \gamma^5 \not{p}_4 p_{4\mu} \frac{1}{2m_{N^*}^0} \frac{P^{\mu\nu}(q)}{E - m_{N^*}^0} \gamma^5 \not{p}_2 p_{2\nu} u(\vec{p}_1, \lambda_1) IF_{N^*s}(I). \quad (\text{A19})$$

$$IF_{N^*s}(1/2) = 1.$$

6. $\eta N \rightarrow \rho N$

- $N^*(S_{11})$ pole diagram

$$-i\kappa \frac{f_{N^*N\eta} g_{N^*N\rho}}{m_\pi} \bar{u}(\vec{p}_3, \lambda_3) \gamma^5 \not{\xi}^*(\vec{p}_4, \lambda_4) \frac{1}{2m_{N^*}^0} \frac{\not{q} + m_{N^*}^0}{E - m_{N^*}^0} \not{p}_2 u(\vec{p}_1, \lambda_1) IF_{N^*s}(I). \quad (\text{A20})$$

- $N^*(D_{13})$ pole diagram

$$i\kappa \frac{f_{N^*N\eta} f_{N^*N\rho}}{m_\pi^2 m_\rho} \bar{u}(\vec{p}_3, \lambda_3) (\not{p}_4 \epsilon_\mu^*(\vec{p}_4, \lambda_4) - p_{4\mu} \not{\xi}^*(\vec{p}_4, \lambda_4)) \frac{P^{\mu\nu}(q)}{2m_{N^*}^0 (E - m_{N^*}^0)} p_{2\nu} \gamma^5 \not{p}_2 u(\vec{p}_1, \lambda_1) IF_{N^*s}(I) \quad (\text{A21})$$

$$IF_{N^*s}(1/2) = \sqrt{3}.$$

7. $\eta N \rightarrow \pi \Delta$

- $N^*(S_{11})$ pole diagram

$$\kappa \frac{f_{N^*N\eta} f_{N^*\Delta\pi}}{m_\pi^2} \bar{u}_\mu(\vec{p}_3, \lambda_3) p_4^\mu \gamma^5 \frac{1}{2m_{N^*}^0} \frac{\not{q} + m_{N^*}^0}{E - m_{N^*}^0} \not{p}_2 u(\vec{p}_1, \lambda_1) IF_{N^*s}(I). \quad (\text{A22})$$

- $N^*(P_{13})$ pole diagram

$$\kappa \frac{f_{N^*N\eta} f_{N^*\Delta\pi}}{m_\pi^2} \bar{u}_\mu(\vec{p}_3, \lambda_3) \gamma^5 \not{p}_4 \frac{1}{2m_{N^*}^0} \frac{P^{\mu\nu}(q)}{E - m_{N^*}^0} p_{2\nu} u(\vec{p}_1, \lambda_1) IF_{N^*s}(I). \quad (\text{A23})$$

- $N^*(D_{13})$ pole diagram

$$-\kappa \frac{f_{N^*N\eta} f_{N^*\Delta\pi}}{m_\pi^3} \bar{u}_\mu(\vec{p}_3, \lambda_3) \not{p}_4 \frac{1}{2m_{N^*}^0} \frac{P^{\mu\nu}(q)}{E - m_{N^*}^0} \gamma^5 \not{p}_2 p_{2\nu} u(\vec{p}_1, \lambda_1) IF_{N^*s}(I). \quad (\text{A24})$$

$$IF_{N^*s}(1/2) = -\sqrt{2}.$$

8. $\rho N \rightarrow \rho N$

- $N^*(S_{11})$ pole diagram

$$\kappa g_{N^*N\rho}^2 \bar{u}(\vec{p}_3, \lambda_3) \gamma^5 \xi^*(\vec{p}_4, \lambda_4) \frac{1}{2m_{N^*}^0} \frac{\not{p}_4 + m_{N^*}^0}{E - m_{N^*}^0} \gamma^5 \xi(\vec{p}_2, \lambda_2) u(\vec{p}_1, \lambda_1) IF_{N^*s}(I). \quad (\text{A25})$$

- $N^*(D_{13}, D_{33})$ pole diagrams

$$\begin{aligned} & \kappa \frac{f_{N^*N\rho}^2}{m_\rho^2} \bar{u}(\vec{p}_3, \lambda_3) (\not{p}_4 \epsilon^*(\vec{p}_4, \lambda_4) - p_{4\mu} \xi^*(\vec{p}_4, \lambda_4)) \\ & \times \frac{P^{\mu\nu}(q)}{2m_{N^*}(E - m_{N^*}^0)} (\not{p}_2 \epsilon_\nu^*(\vec{p}_2, \lambda_2) - p_{2\nu} \xi^*(\vec{p}_2, \lambda_2)) u(\vec{p}_1, \lambda_1) IF_{N^*s}(I) \quad (\text{A26}) \\ IF_{N^*s}(1/2) &= 3, IF_{N^*s}(3/2) = 1. \end{aligned}$$

9. $\rho N \rightarrow \pi \Delta$

- $N^*(D_{13}, D_{33})$ pole diagrams

$$\begin{aligned} & i\kappa \frac{f_{N^*N\rho} f_{N^*\Delta\pi}}{m_\pi m_\rho} \bar{u}_\mu(\vec{p}_3, \lambda_3) \not{p}_4 \\ & \times \frac{P^{\mu\nu}(q)}{2m_{N^*}(E - m_{N^*}^0)} (\not{p}_2 \epsilon_\nu^*(\vec{p}_2, \lambda_2) - p_{2\nu} \xi^*(\vec{p}_2, \lambda_2)) u(\vec{p}_1, \lambda_1) IF_{N^*s}(I) \quad (\text{A27}) \\ IF_{N^*s}(1/2) &= -\sqrt{6}, IF_{N^*s}(3/2) = \sqrt{\frac{5}{3}}. \end{aligned}$$

10. $\pi \Delta \rightarrow \pi \Delta$

- $N^*(S_{11}, S_{31})$ pole diagrams

$$-\kappa \frac{f_{N^*\Delta\pi}^2}{m_\pi^2} \bar{u}_\mu(\vec{p}_3, \lambda_3) p_4^\mu \gamma^5 \frac{1}{2m_{N^*}^0} \frac{\not{p}_4 + m_{N^*}^0}{E - m_{N^*}^0} \gamma^5 p_2^\nu u_\nu(\vec{p}_1, \lambda_1) IF_{N^*s}(I). \quad (\text{A28})$$

- $N^*(P_{31})$ pole diagram

$$\kappa \frac{f_{N^*\Delta\pi}^2}{m_\pi^2} \bar{u}_\mu(\vec{p}_3, \lambda_3) p_4^\mu \frac{1}{2m_{N^*}^0} \frac{\not{p}_4 + m_{N^*}^0}{E - m_{N^*}^0} p_2^\nu u_\nu(\vec{p}_1, \lambda_1) IF_{N^*s}(I). \quad (\text{A29})$$

- $N^*(P_{13})$ pole diagram

$$\kappa \frac{f_{N^*\Delta\pi}^2}{m_\pi^2} \bar{u}_\mu(\vec{p}_3, \lambda_3) \gamma^5 \not{p}_4 \frac{1}{2m_{N^*}^0} \frac{P^{\mu\nu}(q)}{E - m_{N^*}^0} \gamma^5 \not{p}_2 u_\nu(\vec{p}_1, \lambda_1) IF_{N^*s}(I). \quad (\text{A30})$$

- $N^*(D_{13}, D_{33})$ pole diagrams

$$\begin{aligned} & \kappa \frac{f_{N^*\Delta\pi}^2}{m_\pi^2} \bar{u}_\mu(\vec{p}_3, \lambda_3) \not{p}_4 \frac{1}{2m_{N^*}^0} \frac{P^{\mu\nu}(q)}{E - m_{N^*}^0} \not{p}_2 u_\nu(\vec{p}_1, \lambda_1) IF_{N^*s}(I). \quad (\text{A31}) \\ IF_{N^*s}(1/2) &= 2, IF_{N^*s}(3/2) = \frac{5}{3}. \end{aligned}$$

-
- [1] R. Koch, Z. Phys. **C 29**, 597 (1985).
- [2] R.A. Arndt, I.I. Strakovsky, R.L. Workman and M.M. Pavan, Phys. Rev. C **52**, 2120 (1995).
- [3] R.A. Arndt, R.L. Workman, I.I. Strakovsky and M.M. Pavan, nucl-th/9807087 (1998).
- [4] M. Mojžiš, Eur. Phys. J. C **2**, 181 (1998).
- [5] N. Fettes and U. Meißner, Nucl. Phys. **A693**, 693 (2001).
- [6] B.C. Pearce and B.K. Jennings, Nucl. Phys. **A528**, 655 (1991).
- [7] F. Gross and Y. Surya, Phys. Rev. C **47**, 703 (1993).
- [8] O. Krehl, C. Hanhart, S. Krewald and J. Speth, Phys. Rev. C **62**, 025207 (2000).
- [9] H. Machner and J. Haidenbauer, J. Phys. G **25**, R231 (1999).
- [10] P. Moskal, M. Wolke, A. Khoukaz, and W. Oelert, Prog. Part. Nucl. Phys. **49**, 1 (2002).
- [11] E. Hernández and E. Oset, Phys. Lett. B **350**, 158 (1995).
- [12] C. Hanhart, J. Haidenbauer, A. Reuber, C. Schütz and J. Speth, Phys. Lett. B **358**, 21 (1995).
- [13] C. Hanhart, J. Haidenbauer, O. Krehl and J. Speth, Phys. Lett. B **444**, 25 (1998).
- [14] M. Batinić and A. Švarc, Phys. Scr. **56**, 321 (1997).
- [15] G. Fäldt and C. Wilkin, Phys. Scr. **64**, 427 (2001).
- [16] K. Nakayama, J. Speth, and T.-S.H. Lee, Phys. Rev. C **65**, 045210 (2002).
- [17] V. Baru, A.M. Gasparyan, J. Haidenbauer, C. Hanhart, A.E. Kudryavtsev, and J. Speth, Phys. Rev. C **67**, 024002 (2003).
- [18] K. Nakayama, A. Szczurek, C. Hanhart, J. Haidenbauer and J. Speth, Phys. Rev. C **57**, 1580 (1998).
- [19] K. Tsushima and K. Nakayama, *nucl-th/0304017*.
- [20] A. Gasparian, J. Haidenbauer, C. Hanhart, L. Kondratyuk, and J. Speth, Phys. Lett. B **480**, 273 (2000).
- [21] R. Shyam, G. Penner, and U. Mosel, Phys. Rev. C **63**, 022202 (2001).
- [22] C. Schütz, J.W. Durso, K. Holinde and J. Speth, Phys. Rev. C **49**, 2671 (1994).
- [23] C. Schütz, K. Holinde, J. Speth, B.C. Pearce and J.W. Durso, Phys. Rev. C **51**, 1374 (1995).
- [24] C. Schütz, J. Haidenbauer, J.W. Durso and J. Speth, Phys. Rev. C **57**, 1464 (1998).
- [25] O. Krehl, C. Hanhart, S. Krewald, and J. Speth, Phys. Rev. C **60**, 055206 (1999).
- [26] A.B. Gridnev and N.G. Kozlenko, Eur. Phys. J. A **4**, 187 (1999).
- [27] G. Penner and U. Mosel, Phys. Rev. C **66**, 055211 (2002).
- [28] V. Shklyar, G. Penner, and U. Mosel, *hep-th/0301152*.
- [29] K. Hagiwara et al., Phys. Rev. D **66**, 010001 (2002).
- [30] R. Aaron, R.D. Amado and J.E. Young., Phys. Rev. **174**, 2022 (1968).
- [31] A. Müller-Groeling, K. Holinde and J. Speth, Nucl. Phys. **A513**, 557 (1990).
- [32] J. Wess and B. Zumino, Phys. Rev. **163**, 1727 (1967).
- [33] V. Bernard, N. Kaiser, and U.-G. Meissner, Nucl. Phys. **A615**, 483 (1997).
- [34] K. Erkelenz, Phys. Rep. **C13**, 191 (1974).
- [35] R. Aaron and R.D. Amado, Phys. Rev. **150**, 857 (1966).
- [36] R.T. Cahill and I.H. Sloan, Nucl. Phys. **A165**, 161 (1971).
- [37] J.W. Durso, A.D. Jackson and B.J. Verwest, Nucl. Phys. **A345**, 471 (1980).
- [38] C. Caso et al., Eur. Phys. J. C **3**, 1 (1998).
- [39] A. Gasparyan, *PhD thesis, Jülich Report, No. 4015 (2002)*.
- [40] S. Weinberg, Phys. Rev. Lett. **17**, 616 (1966).

- [41] Y. Tomozawa, *Nuovo Cim.* **46A**, 707 (1966).
- [42] G. Penner and U. Mosel, *Phys. Rev. C* **65**, 055202 (2002).
- [43] T. Inoue, E. Oset, M.J. Vicente Vacas, *Phys. Rev. C* **65**, 035204 (2002).
- [44] C. Hanhart and K. Nakayama, *Phys. Lett. B* **454**, 176 (1999).
- [45] O. Krehl and J. Speth, *Acta Phys. Polon. B* **29**, 2477 (1998).
- [46] A. Sibirtsev, S. Schneider, C. Elster, J. Haidenbauer, S. Krewald and J. Speth, *Phys. Rev. C* **65**, 044007 (2002).
- [47] V.Yu. Grishina, L.A. Kondratyuk, M. Büscher, J. Haidenbauer, C. Hanhart, and J. Speth, *Phys. Lett.* **B475**, 9 (2000).
- [48] H. Garcilazo and M. T. Peña, *Phys. Rev. C* **66**, 034606 (2002).
- [49] W.R. Frazer and J.R. Fulco, *Phys. Rev.* **117**, 1603 (1960).
- [50] R. Koch, *Nucl. Phys. A* **448**, 707 (1986).
- [51] R.M. Brown et al., *Nucl. Phys.* **B153**, 89 (1979).
- [52] F. Bulos et al., *Phys. Rev. Lett.* **13**, 486 (1964).
- [53] F. Bulos et al., *Phys. Rev.* **187**, 1827 (1969).
- [54] W. Deinet et al., *Nucl. Phys.* **B11**, 495 (1969).
- [55] J. Feltesse et al., *Nucl. Phys.* **B93**, 242 (1975).
- [56] B.W. Richards et al., *Phys. Rev. D* **1**, 10 (1970).
- [57] T. Morrison, *Ph.D. thesis, The George Washington University, 1999.*
- [58] N.C. Debenham et al., *Phys. Rev. D* **12**, 2545 (1975).
- [59] G. Janßen, K. Holinde and J. Speth, *Phys. Rev. C* **54**, 2218 (1996).
- [60] J.W. Durso, *Phys. Lett. B* **184**, 348 (1987).
- [61] C. Schütz, *PhD thesis, Jülich Report, No. 3130 (1995).*
- [62] G.E. Brown and W. Weise, *Phys. Rep.* **22**, 279 (1975).
- [63] G. Janßen, B.C. Pearce, K. Holinde and J. Speth, *Phys. Rev. D* **52**, 2690 (1995).
- [64] O. Krehl and J. Speth, *Nucl. Phys.* **A623**, 162c (1997).
- [65] R. Koch and E. Pietarinen, *Nucl. Phys.* **A336**, 331 (1980).

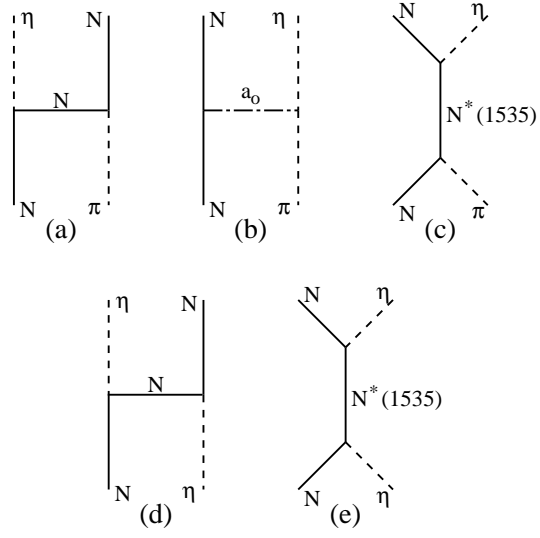


FIG. 1: Contribution to the elastic πN channel.

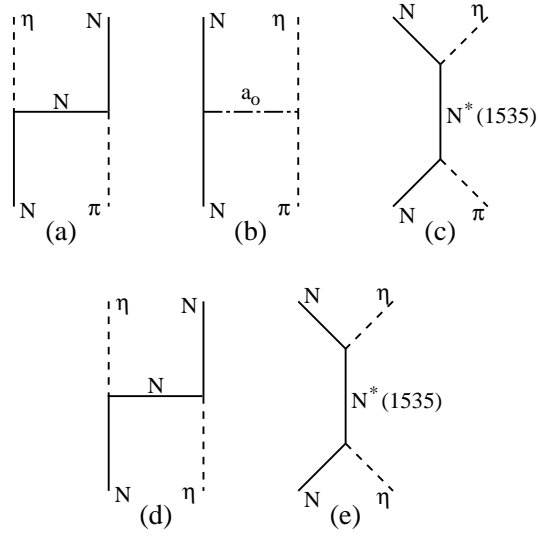


FIG. 2: Contribution to the $\pi N \rightarrow \eta N$ transition and to the ηN channel.

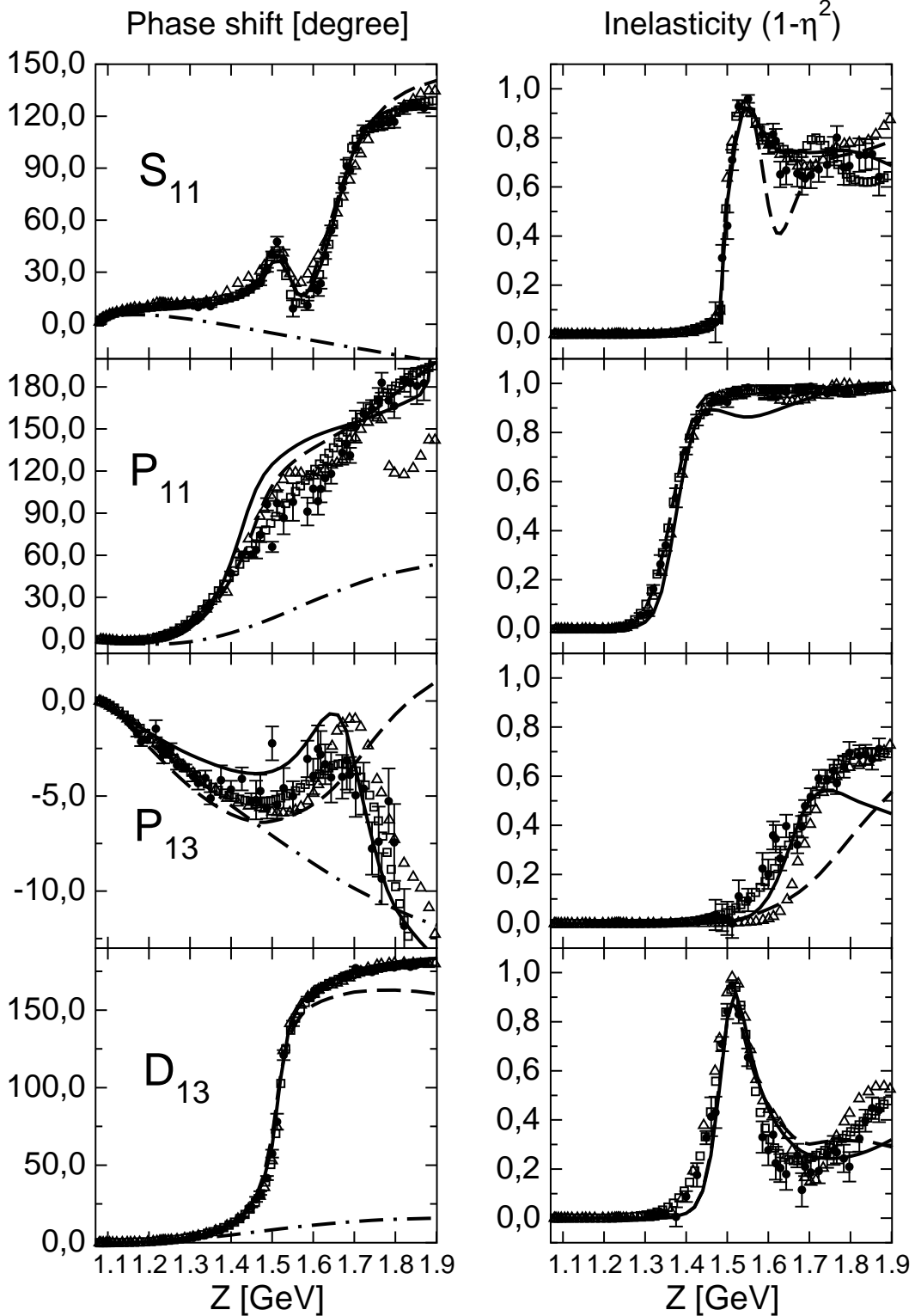


FIG. 3: The πN phase shifts and inelasticities for the isospin $I = 1/2$ partial waves. The dashed curves show the results of the πN model of O. Krehl et al. [8]. The dash-dotted curves represent the results based on the background contributions of our new model, as discussed in the text. The results of the full model are given by the solid lines. The data are from the phase shift analyses KA84[50], SM95[2], and SE-SM95[2].

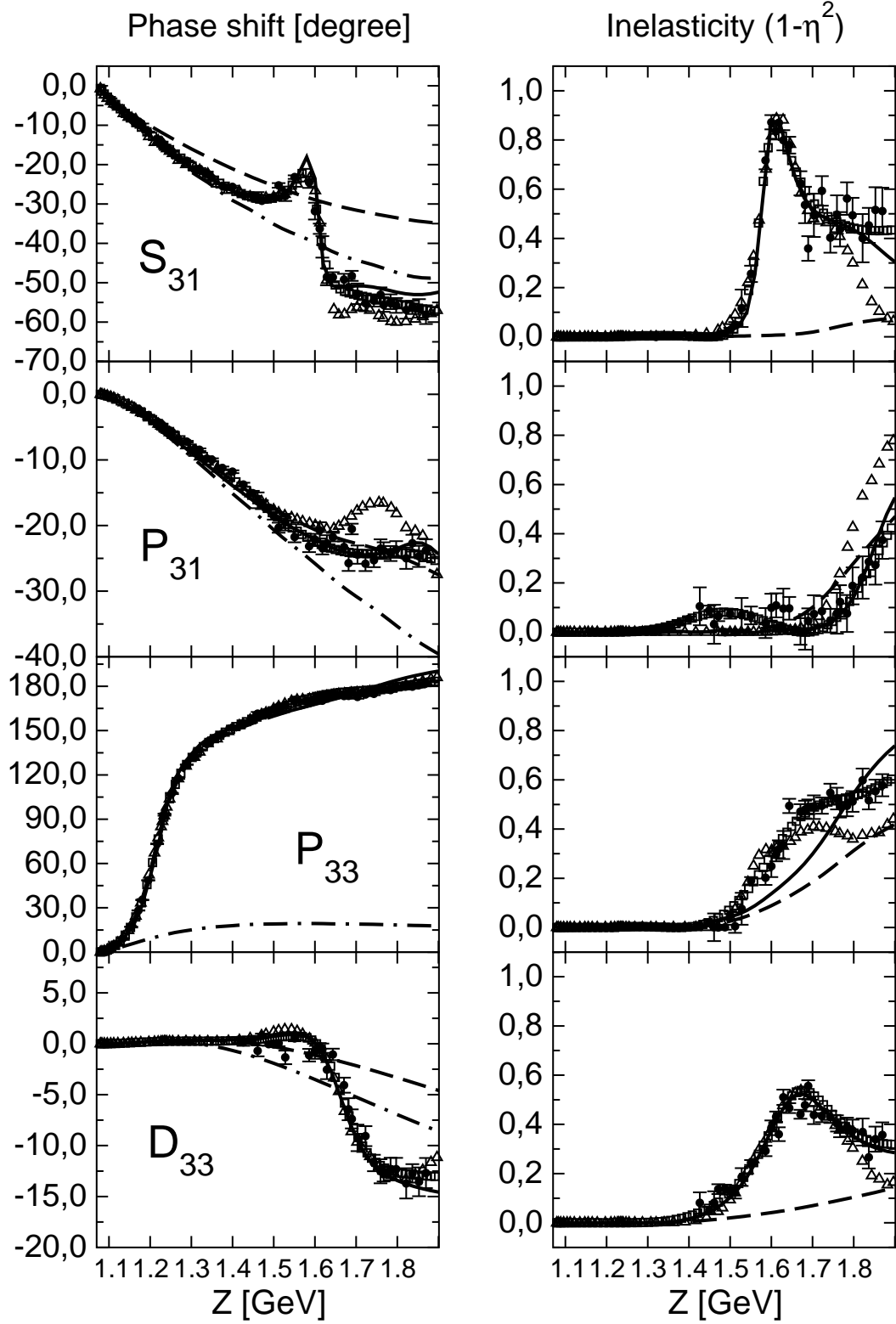


FIG. 4: The πN phase shifts and inelasticities for the isospin $I = 3/2$ partial waves. Same description of curves and experiments as in fig. 3.

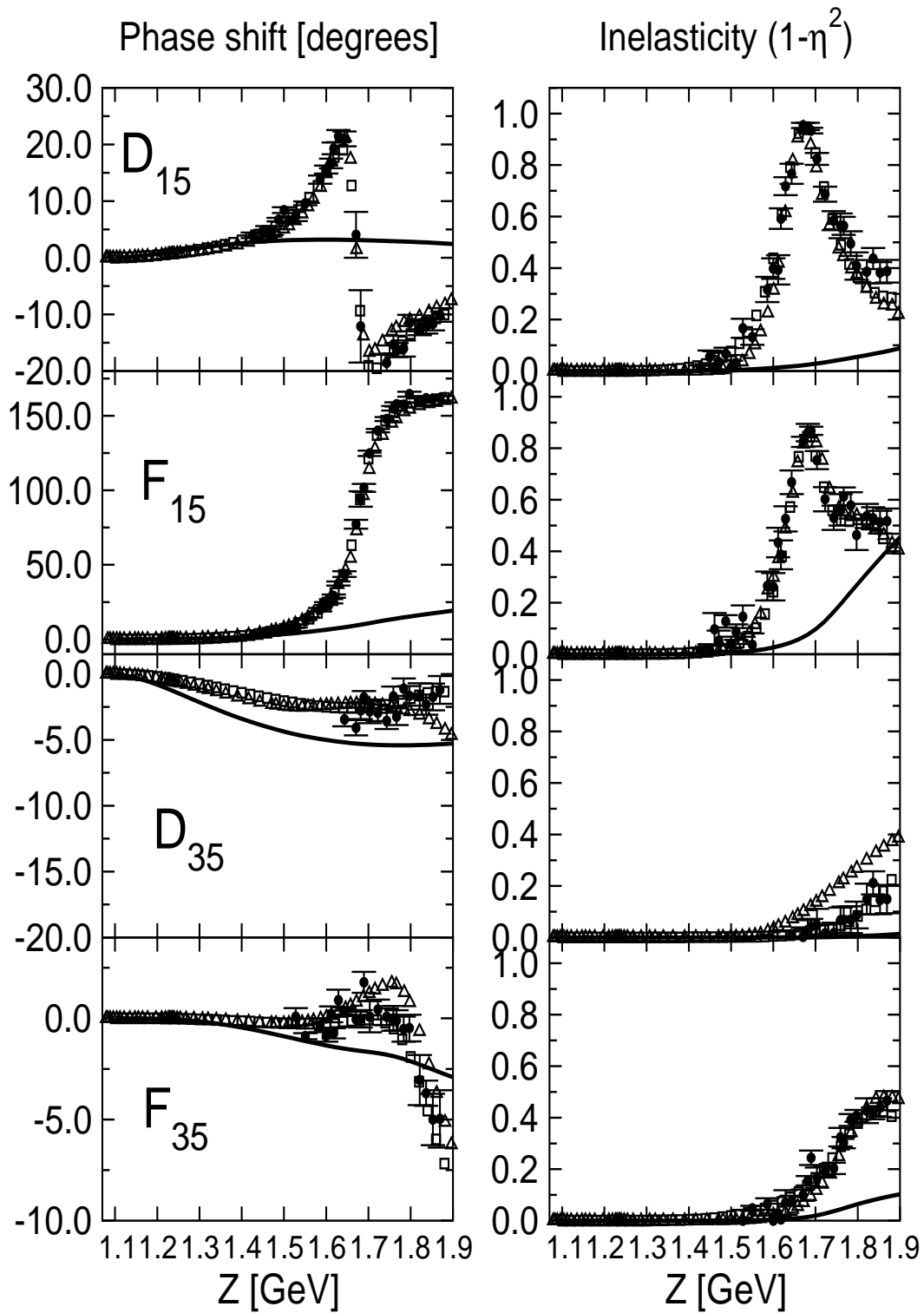


FIG. 5: Phase shifts and inelasticity for πN partial waves with $J = 5/2$. Same description of curves and experiments as in fig. 3.

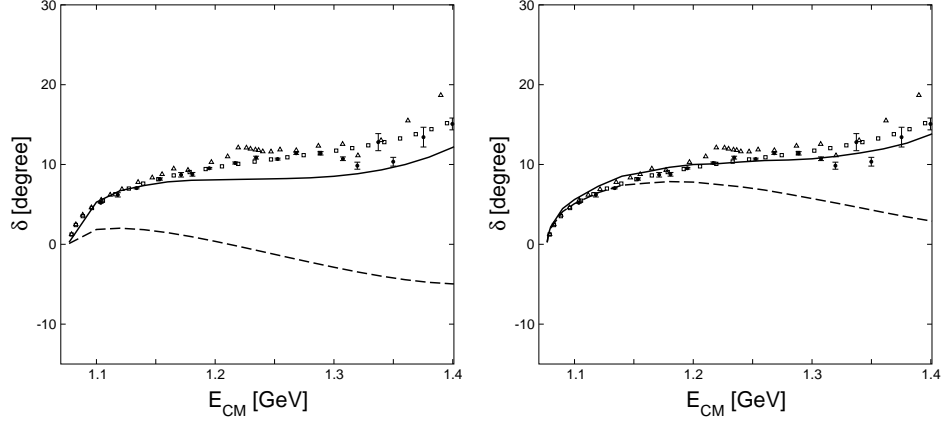


FIG. 6: πN phase shift in the S_{11} partial wave. The results of the model of Krehl et al. [8] are shown on the left side, those of the new model on the right side. The curves correspond to the full model (solid line) and to the full model with the contribution of the $S_{11}(1650)$ resonance switched off (dashed line). The data are from the phase shift analyses KA84 [50], SM95 [2], and SE-SM95 [2].

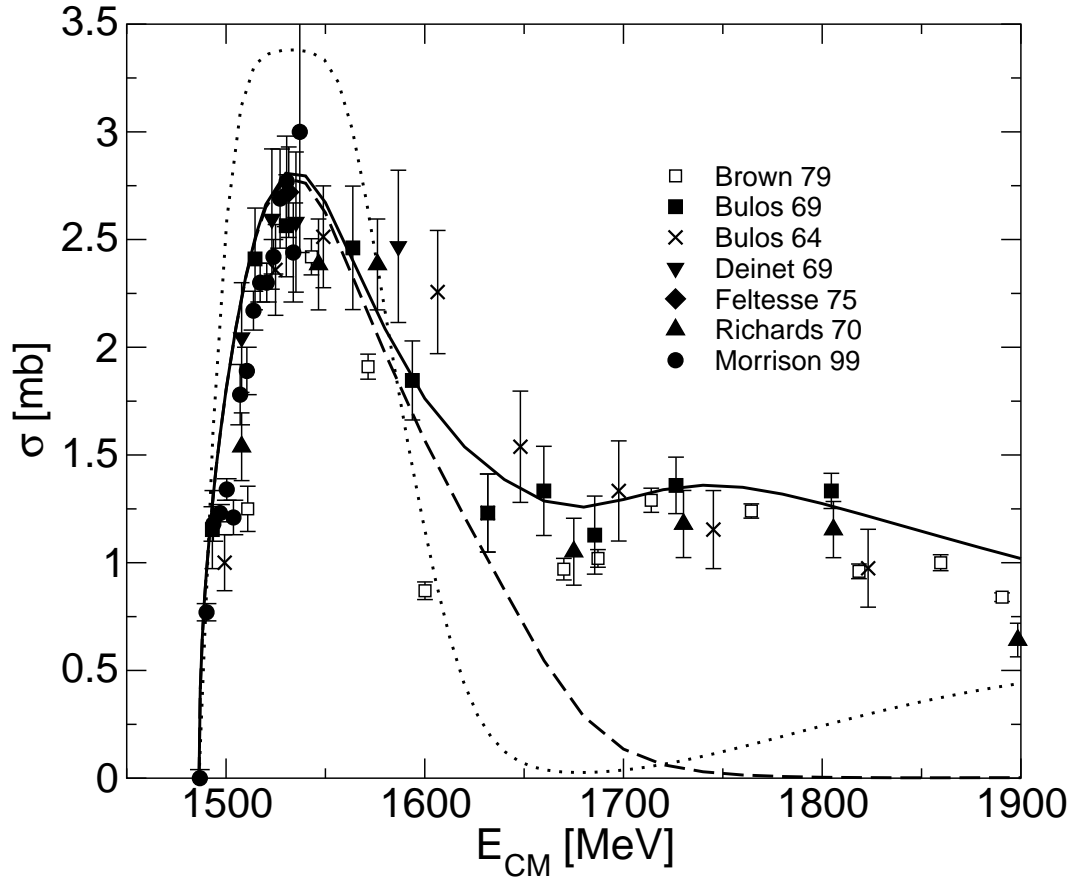


FIG. 7: $\pi^-p \rightarrow \eta n$ total cross section. The solid line corresponds to the full calculation. The dashed line indicates the pure s -wave contribution. The results of the old model are shown as a dotted line (only s -wave). The data are from Refs. [51, 52, 53, 54, 55, 56, 57].

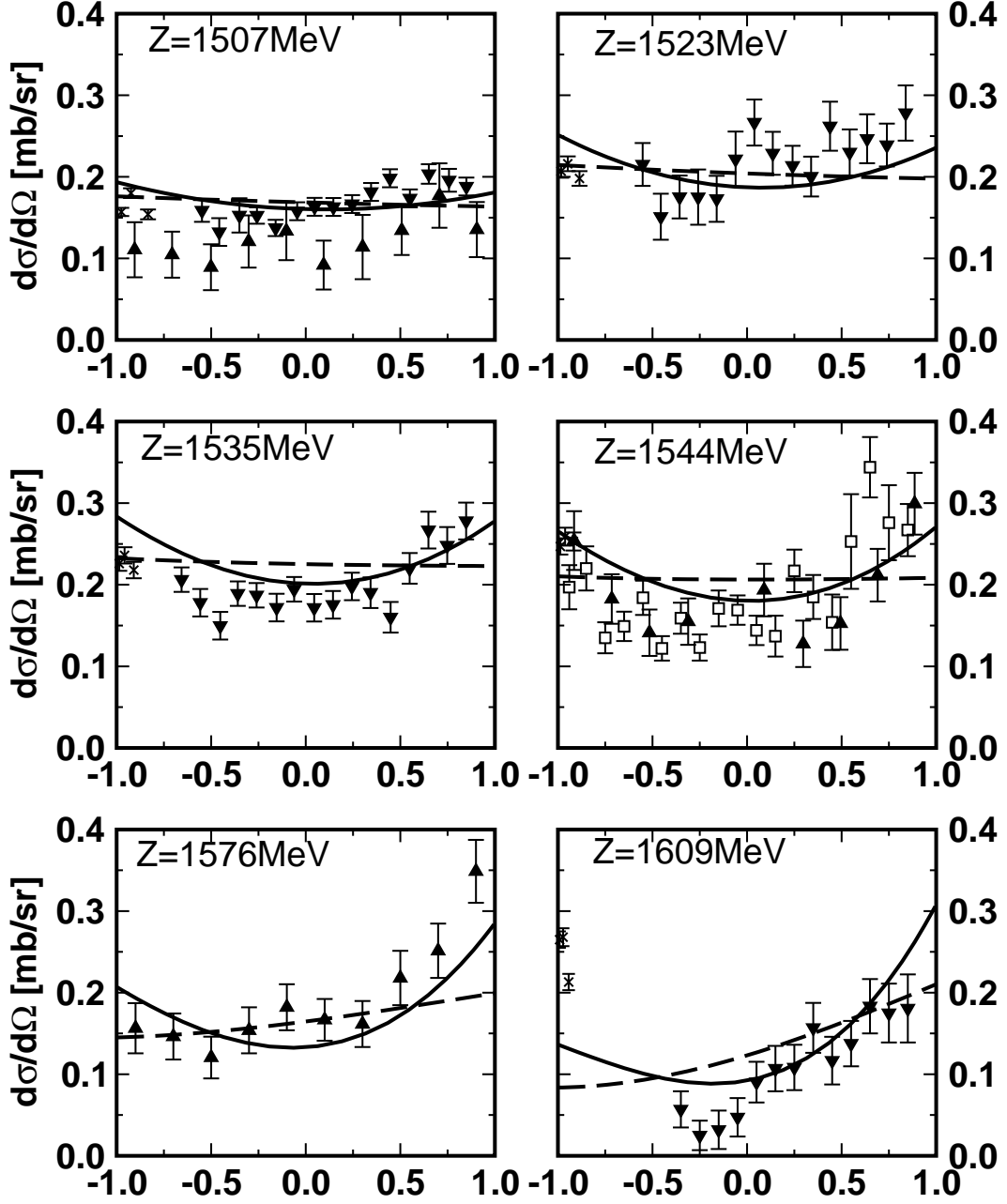


FIG. 8: $\pi^- N \rightarrow \eta n$ differential cross section at energies close to the ηN threshold. The solid curve corresponds to the full result. The dashed line corresponds to the case when the D_{13} partial wave is switched off. The data are from [51](\square), [54](\blacktriangledown), [56](\blacktriangle), [58](\times).

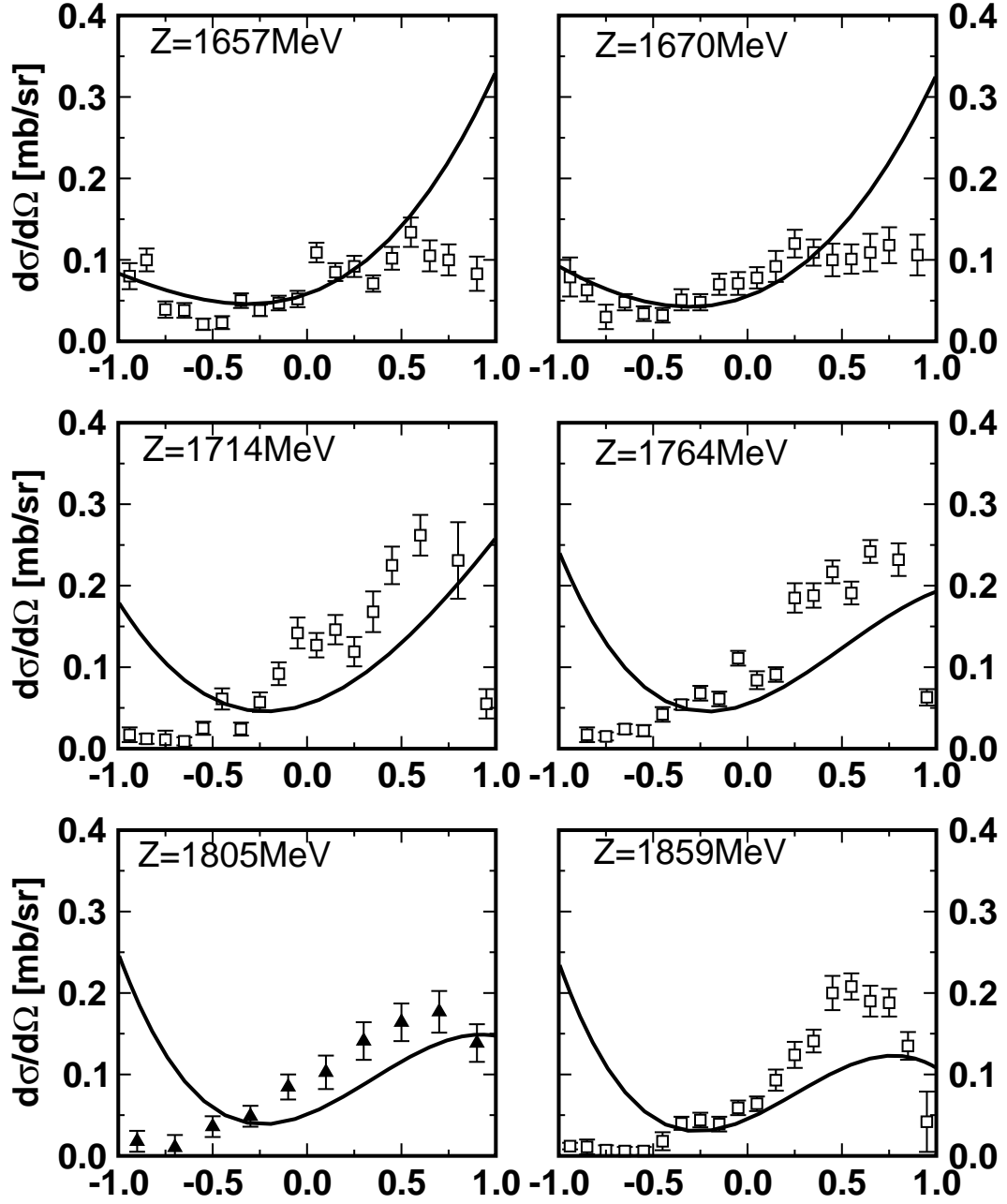


FIG. 9: $\pi^- N \rightarrow \eta n$ differential cross section at higher energies. The data are from [51](\square), [54](\blacktriangledown), [56](\blacktriangle), [58](\times).

Vertex	\mathcal{L}_{int}
$NN\pi$	$-\frac{f_{NN\pi}}{m_\pi}\bar{\Psi}\gamma^5\gamma^\mu\vec{\tau}\partial_\mu\vec{\pi}\Psi$
$N\Delta\pi$	$\frac{f_{N\Delta\pi}}{m_\pi}\bar{\Delta}^\mu\vec{S}^\dagger\partial_\mu\vec{\pi}\Psi + \text{h.c.}$
$\rho\pi\pi$	$-g_{\rho\pi\pi}(\vec{\pi}\times\partial_\mu\vec{\pi})\vec{\rho}^\mu$
$NN\rho$	$-g_{NN\rho}\bar{\Psi}[\gamma^\mu - \frac{\kappa_\rho}{2m_N}\sigma^{\mu\nu}\partial_\nu]\vec{\tau}\vec{\rho}_\mu\Psi$
$NN\sigma$	$-g_{NN\sigma}\bar{\Psi}\Psi\sigma$
$\sigma\pi\pi$	$\frac{g_{\sigma\pi\pi}}{2m_\pi}\partial_\mu\vec{\pi}\partial^\mu\vec{\pi}\sigma$
$\sigma\sigma\sigma$	$-g_{\sigma\sigma\sigma}m_\sigma\sigma\sigma\sigma$
$NN\rho\pi$	$\frac{f_{NN\pi}}{m_\pi}g_\rho\bar{\Psi}\gamma^5\gamma^\mu\vec{\tau}\Psi(\vec{\rho}_\mu\times\vec{\pi})$
NNa_1	$-\frac{f_{NN\pi}}{m_\pi}m_{a_1}\bar{\Psi}\gamma^5\gamma^\mu\vec{\tau}\Psi\vec{a}_\mu$
$a_1\pi\rho$	$-\frac{g_\rho}{m_{a_1}}[\partial_\mu\vec{\pi}\times\vec{a}_\nu - \partial_\nu\vec{\pi}\times\vec{a}_\mu][\partial^\mu\vec{\rho}^\nu - \partial^\nu\vec{\rho}^\mu]$ $+\frac{g_\rho}{2m_{a_1}}[\vec{\pi}\times(\partial_\mu\vec{\rho}_\nu - \partial_\nu\vec{\rho}_\mu)][\partial^\mu\vec{a}^\nu - \partial^\nu\vec{a}^\mu]$
$NN\omega$	$-g_{NN\omega}\bar{\Psi}\gamma^\mu\omega_\mu\Psi$
$\omega\pi\rho$	$\frac{g_{\omega\pi\rho}}{m_\omega}\epsilon_{\alpha\beta\mu\nu}\partial^\alpha\vec{\rho}^\beta\partial^\mu\vec{\pi}\omega^\nu$
$N\Delta\rho$	$-i\frac{f_{N\Delta\rho}}{m_\rho}\bar{\Delta}^\mu\gamma^5\gamma^\nu\vec{S}^\dagger\vec{\rho}_{\mu\nu}\Psi + \text{h.c.}^a$
$\rho\rho\rho$	$\frac{g_\rho}{2}(\vec{\rho}_\mu\times\vec{\rho}_\nu)\vec{\rho}^{\mu\nu}$
$NN\rho\rho$	$\frac{\kappa_\rho g_\rho^2}{8m_N}\bar{\Psi}\sigma^{\mu\nu}\vec{\tau}\Psi(\vec{\rho}_\mu\times\vec{\rho}_\nu)$
$\Delta\Delta\pi$	$\frac{f_{\Delta\Delta\pi}}{m_\pi}\bar{\Delta}_\mu\gamma^5\gamma^\nu\vec{T}\Delta^\mu\partial_\nu\vec{\pi}$
$\Delta\Delta\rho$	$-g_{\Delta\Delta\rho}\bar{\Delta}_\tau(\gamma^\mu - i\frac{\kappa_{\Delta\Delta\rho}}{2m_\Delta}\sigma^{\mu\nu}\partial_\nu)\vec{\rho}_\mu\vec{T}\Delta^\tau$
$NN\eta$	$-\frac{f_{NN\eta}}{m_\pi}\bar{\Psi}\gamma^5\gamma^\mu\partial_\mu\eta\Psi$
NNa_0	$g_{NNa_0}m_\pi\bar{\Psi}\vec{\tau}\Psi\vec{a}_0$
$\pi\eta a_0$	$g_{\pi\eta a_0}m_\pi\eta\vec{\pi}\vec{a}_0$
$N^*(S_{11})N\pi$	$\frac{f_{N^*N\pi}}{m_\pi}\bar{\Psi}_{N^*}\gamma^\mu\vec{\tau}\Psi\partial_\mu\vec{\pi} + \text{h.c.}$
$N^*(S_{11})N\eta$	$\frac{f_{N^*N\eta}}{m_\pi}\bar{\Psi}_{N^*}\gamma^\mu\Psi\partial_\mu\eta + \text{h.c.}$
$N^*(S_{11})N\rho$	$g_{N^*N\rho}\bar{\Psi}_{N^*}\gamma^5\gamma^\mu\vec{\tau}\vec{\rho}_\mu\Psi + \text{h.c.}$
$N^*(S_{11})\Delta\pi$	$-\frac{f_{N^*\Delta\pi}}{m_\pi}\bar{\Psi}_{N^*}\gamma^5\vec{S}\Delta^\mu\partial_\mu\vec{\pi} + \text{h.c.}$
$N^*(P_{13})N\pi$	$\frac{f_{N^*N\pi}}{m_\pi}\bar{\Psi}_{N^*}\vec{\tau}\Psi\partial_\mu\vec{\pi} + \text{h.c.}$
$N^*(P_{13})N\eta$	$\frac{f_{N^*N\eta}}{m_\pi}\bar{\Psi}_{N^*}^\mu\Psi\partial_\mu\eta + \text{h.c.}$
$N^*(P_{13})\Delta\pi$	$\frac{f_{N^*\Delta\pi}}{m_\pi}\bar{\Psi}_{N^*}^\mu\gamma^5\gamma^\nu\vec{S}\Delta_\mu\partial_\nu\vec{\pi} + \text{h.c.}$
$N^*(D_{13})N\pi$	$\frac{f_{N^*N\pi}}{m_\pi^2}\bar{\Psi}\gamma^5\gamma^\nu\vec{\tau}\Psi_{N^*}^\mu\partial_\nu\partial_\mu\vec{\pi} + \text{h.c.}$
$N^*(D_{13})N\eta$	$\frac{f_{N^*N\eta}}{m_\pi^2}\bar{\Psi}\gamma^5\gamma^\nu\Psi_{N^*}^\mu\partial_\nu\partial_\mu\eta + \text{h.c.}$
$N^*(D_{13})\Delta\pi$	$i\frac{f_{N^*\Delta\pi}}{m_\pi}\bar{\Psi}_{N^*\nu}\vec{S}\gamma^\mu\Delta^\nu\partial_\mu\vec{\pi} + \text{h.c.}$
$N^*(D_{13})N\rho$	$\frac{f_{N^*N\rho}}{m_\rho}\bar{\Psi}_{N^*}^\mu\gamma^\nu\vec{\tau}\vec{\rho}_{\mu\nu}\Psi + \text{h.c.}$
$\Delta^*(S_{31})N\pi$	$\frac{f_{\Delta^*N\pi}}{m_\pi}\bar{\Delta}^*\gamma^\mu\vec{S}^\dagger\Psi\partial_\mu\vec{\pi} + \text{h.c.}$
$\Delta^*(S_{31})\Delta\pi$	$-\frac{f_{\Delta^*\Delta\pi}}{m_\pi}\bar{\Delta}^*\gamma^5\vec{T}\Delta^\mu\partial_\mu\vec{\pi} + \text{h.c.}$
$\Delta^*(P_{31})N\pi$	$-\frac{f_{\Delta^*N\pi}}{m_\pi}\bar{\Delta}^*\gamma^5\gamma^\mu\vec{S}^\dagger\Psi\partial_\mu\vec{\pi} + \text{h.c.}$
$\Delta^*(P_{31})\Delta\pi$	$-\frac{f_{\Delta^*\Delta\pi}}{m_\pi}\bar{\Delta}^*\vec{T}\Delta^\mu\partial_\mu\vec{\pi} + \text{h.c.}$
$N^*(D_{33})N\pi$	$\frac{f_{N^*N\pi}}{m_\pi^2}\bar{\Psi}\gamma^5\gamma^\nu\vec{S}^\dagger\Psi_{N^*}^\mu\partial_\nu\partial_\mu\vec{\pi} + \text{h.c.}$
$N^*(D_{33})\Delta\pi$	$i\frac{f_{N^*\Delta\pi}}{m_\pi}\bar{\Delta}^*\nu\vec{T}\gamma^\mu\Delta^\nu\partial_\mu\vec{\pi} + \text{h.c.}$
$N^*(D_{33})N\rho$	$\frac{f_{N^*N\rho}}{m_\rho}\bar{\Delta}^*\gamma^\nu\vec{S}^\dagger\vec{\rho}_{\mu\nu}\Psi + \text{h.c.}$

TABLE I: The effective Lagrangian

Mesons		Baryons
m_π 138.03	m_ω 782.6	m_N 938.926
m_η 547.45	m_{a_0} 982.7	m_Δ 1232.0
m_σ 650.0	m_{a_1} 1260.0	
m_ρ 769.0		

TABLE II: Masses of mesons and baryons (in MeV) used in the calculations.

Vertex	Type of the diagram	Coupling constant	Ref.	Cutoff Λ [MeV]
correlated $\pi\pi$ -exchange:				
	ρ -channel			1000
	σ -channel	$A_0 = \mathbf{25} \text{ MeV}/F_\pi^2$		900
$NN\pi$	N exchange	$\frac{f_{NN\pi}^2}{4\pi} = 0.0778$	[59]	1100
$N\Delta\pi$	Δ exchange	$\frac{f_{N\Delta\pi}^2}{4\pi} = 0.36$	[59]	1800
$NN\rho$	N exchange	$\frac{g_{NN\rho}^2}{4\pi} = 0.84$	[59]	1600
		$\kappa = 6.1$	[59]	
$NN\rho\pi$	contact term	$\sim f_{NN\pi}g_{NN\rho}$		1100
$NN\pi$	π exchange	$\sim f_{NN\pi}$		900
$\pi\pi\rho$	π exchange	$\frac{g_{\pi\pi\rho}^2}{4\pi}$		900
$NN\omega$	ω exchange	$\frac{g_{NN\omega}^2}{4\pi} = 11.0$	[59]	1200
$\omega\pi\rho$	ω exchange	$\frac{g_{\omega\pi\rho}^2}{4\pi} = 10.0$	[18, 60]	1200
NNa_1	a_1 exchange	$\sim f_{NN\pi}$		1600
$a_1\pi\rho$	a_1 exchange	$\sim g_{NN\rho}$		1600
$NN\rho$	ρ exchange	$g_{NN\rho}, \kappa$		1400
$\rho\rho\rho$	ρ exchange	$\sim g_{NN\rho}$		1400
$NN\rho\rho$	contact term	$\sim g_{NN\rho}^2\kappa$		1200
$N\Delta\pi$	N exchange	$\frac{f_{N\Delta\pi}^2}{4\pi} = 0.36$	[59]	1600
$\Delta\Delta\pi$	Δ exchange	$\frac{f_{\Delta\Delta\pi}^2}{4\pi} = 0.252$	[61, 62]	1800
$N\Delta\rho$	ρ exchange	$\frac{f_{N\Delta\rho}^2}{4\pi} = 20.45$	[59]	1400
$\Delta\Delta\rho$	ρ exchange	$\frac{g_{\Delta\Delta\rho}^2}{4\pi} = 4.69,$	[61, 62]	1400
		$\frac{g_{\Delta\Delta\rho}^2}{V} = 6.1$	[61, 62]	
$\pi\pi\rho$	ρ exchange	$\frac{g_{\rho\pi\pi}^2}{4\pi} = 2.90$	[63]	1400
$NN\sigma$	N exchange	$\frac{g_{NN\sigma}^2}{4\pi} = 13$	[37]	1800
$\pi\pi\sigma$	π exchange	$\frac{g_{\pi\pi\sigma}^2}{4\pi} = 0.25$	[64]	1050
$NN\sigma$	σ exchange	$\sim g_{NN\sigma}$		1700
$\sigma\sigma\sigma$	σ exchange	$\frac{g_{\sigma\sigma\sigma}^2}{4\pi} = \mathbf{0.275}$		1700
$NN\eta$	N exchange	$\frac{f_{NN\eta}^2}{4\pi} = 0.00934$	[24]	1500
NNa_0	a_0 exchange	$\frac{g_{NNa_0}g_{\pi\eta a_0}}{4\pi} = 8.0$	[24]	1500
$\pi\eta a_0$	a_0 exchange			1500

TABLE III: Parameters of the vertices which enter into the background diagrams. Free parameters are given in boldface.

Resonance	Bare mass [MeV]	$f^2/(4\pi)$			
		πN	$\pi\Delta$	ρN	ηN
$N_{S_{11}}^*$ (1535)	2051	0.00045	1.09(-)		0.0247
$N_{S_{11}}^*$ (1650)	1919	0.0067		0.046 ^a	
$N_{P_{13}}^*$ (1720)	1910	0.0031	0.0085(-)		0.079(-)
$N_{D_{13}}^*$ (1520)	2263	0.00037	0.0118	0.609	0.0008
Δ (1232)	1459	0.163			
$\Delta_{S_{31}}$ (1620)	2419	0.0154	2.91(-)		
$\Delta_{P_{31}}$ (1910)	2121	0.0043	0.007(-)		
$\Delta_{D_{33}}$ (1700)	2252	0.00038	0.03(-)	0.011	

TABLE IV: Parameters of the pole graphs: bare masses and coupling constants. The minus sign in parenthesis indicates that the coupling constant is negative.

	this work	Ref. [65]	SM95 [2]
S_{11}	0.195	0.173 ± 0.003	0.175
S_{31}	-0.110	-0.101 ± 0.004	-0.087
P_{11}	-0.089	-0.081 ± 0.002	-0.068
P_{31}	-0.046	-0.045 ± 0.002	-0.039
P_{13}	-0.031	-0.030 ± 0.002	-0.022
P_{33}	0.209	0.214 ± 0.002	0.209

TABLE V: The s and p -wave πN scattering lengths and volumes in terms of $m_{\pi^+}^{-(2L+1)}$.